# Eddy–Mean Flow Interaction in the Gulf Stream at 68°W. Part II: Eddy Forcing on the Time-Mean Flow

MEGHAN CRONIN*

*Graduate School of Oceanography, University of Rhode Island, Kingston, Rhode Island*

(Manuscript received 23 March 1994, in final form 2 February 1996)

ABSTRACT

Data from the SYNOP 68°W current meter array show a trough pattern in the 26-month mean Gulf Stream path at 68°W and a cyclone in the mean deep flow. In order to determine whether eddies are controlling the speed and direction of the time-mean Gulf Stream flow at 68°W a theory is developed that extends the Eliassen–Palm theory for zonal-mean flows to time-mean flows. The eddy force is evaluated as the three-dimensional divergence of an eddy stress tensor and is equivalent to the eddy advection of momentum $\mathbf{F}_{mom}$ and the rotated divergent eddy stretching potential vorticity flux $\mathbf{F}_{therm}$. The study region at 68°W is characterized by large amplitude trough formation events. It is shown that $\mathbf{F}_{therm}$ is associated with the growth stage of the eddy trough formation events and tends to turn the upper-level time-mean flow southward into the trough pattern and accelerate and "spin up" the deep-layer cyclone; $\mathbf{F}_{mom}$ has a vertically coherent pattern associated with the decay stage of the trough formation events and tends to offset $\mathbf{F}_{therm}$ particularly in the deep layer.

## 1. Introduction

The Gulf Stream has a rich eddy field, with wavelike meanders and convoluted distortions of the path (Halliwell and Mooers 1983; Watts 1983; Cornillon 1986). At most locations the wavelike meanders propagate along the path. However, downstream of Cape Hatteras, at 68°W, meanders often stall and form large amplitude troughs (Watts et al. 1995). As a result, the 7-year mean Gulf Stream surface front (Lee 1994) shows traces of a trough pattern at 68°W, superimposed upon a broad arc between Cape Hatteras and the New England Seamounts.

Recently, as a part of the SYNOP field program, an array of 12 tall current meter moorings centered at 68°W measured the Gulf Stream's temperature and flow fields from June 1988 to August 1990. During the 26-month experiment, six large amplitude troughs formed in the study region. The upper-layer (400 m, 700 m, 1000 m) time-mean path shows a trough pattern consistent with the historical time-mean surface front, which is clearly related to the trough events at this location. Variability in the deep (3500 m) flow at 68°W is dominated by mesoscale anticyclones and cyclones, which appear to be associated with upper-level meander crests and troughs (Watts et al. 1995; Shay et al. 1995; Cronin and Watts 1996). Indeed, the time-mean deep flow in the study region exhibits a cyclone beneath the upper-layer trough axis.

In a companion paper, Cronin and Watts (1996) determine that the potential energy of the mean jet is the dominant source of the eddy energy and therefore conclude that the mean jet at 68°W is baroclinically unstable. Could these eddies, which have been generated by instabilities on the mean jet, in turn cause a trough in the time-mean upper-layer flow and a cyclone in the time-mean deep flow? The fundamental question here is: How do eddies affect the speed and direction of a time-mean jet?

As discussed in the next section, the existing theories of eddy forcing are not suitable for an observational oceanic analysis. Therefore, in section 3 an eddy-forcing theory is developed that can be applied to the SYNOP Gulf Stream data. The theory extends the Eliassen–Palm theory of zonal-mean eddy forcing to time-mean flows. Section 4 describes the SYNOP 68°W Gulf Stream data, and the time-mean eddy forces are evaluated in section 5. The dynamics of time-mean Gulf Stream flow at 68°W are summarized in section 6.

## 2. Background theory

The dynamical analysis presented in this study assumes that the flow is quasigeostrophic (QG), adiabatic, and mechanically unforced. Additionally, temperature $T$ is used as a proxy for density $\rho$ according

* NOAA Pacific Marine Environmental Laboratory Contribution Number 1685.

*Corresponding author address:* Dr. Meghan Cronin, NOAA/PMEL, 7600 Sand Point Way, NE, Bin C15700, Seattle, WA 98115-0070.

to $\rho = \rho_0(1 - \alpha T)$, where $\alpha$ is the effective coefficient of thermal expansion. According to the QG approximation, the Coriolis parameter $f$ and the total flow field $\mathbf{U} = (U, V, w)$ can each be expanded into an $O(1)$ and a small $O(\mathrm{Ro})$ ($\mathrm{Ro} = |U/(f_0 L)| \ll 1$) component:

$$f = f_0 + \beta y \quad |\beta y| \ll |f_0|$$

$$\mathbf{U} = \mathbf{u} + \mathbf{U}_a \quad |\mathbf{U}_a| \ll |\mathbf{u}|$$

$$\mathbf{u} = \frac{1}{f_0 \rho_0} \hat{\mathbf{z}} \times \nabla P, \tag{1}$$

where $(\hat{\mathbf{x}}, \hat{\mathbf{y}}, \hat{\mathbf{z}})$ are the unit vectors directed eastward, northward, and upward, $\nabla$ is the horizontal gradient operator $\nabla = (\hat{\mathbf{x}}\partial/\partial x, \hat{\mathbf{y}}\partial/\partial y)$, $P$ is pressure, $\rho_0$ is the volume-averaged density, $f_0$ is the Coriolis parameter evaluated at some central latitude ($y = 0$), $\beta$ is the gradient in $f$, and $\mathbf{u}$ is the geostrophic velocity. Formally, $|\mathbf{U}_a|/|\mathbf{u}|$ and $|\beta y|/|f_0|$ scale as the Rossby number $\mathrm{Ro} = |u/(f_0 L)| \ll 1$.

Likewise, the temperature field $T$ can be expanded into a field that is purely depth-dependent $\theta$ and a temporally and weakly spatially varying field $\delta T$:

$$T = \theta(z) + \delta T(x, y, z, t) \quad |\nabla \delta T|, |(\delta T)_z| \ll \theta_z, \tag{2}$$

where the vertical temperature gradient ratio scales as the Rossby number: $|(\delta T)_z|/|\theta_z| \sim \mathrm{Ro} \ll 1$, while the ratio of the horizontal and vertical gradients scales as the product of the aspect ratio and Rossby number: $|\nabla \delta T|/|\theta_z| \sim \mathrm{Ro} H/L \ll 1$.

### *a. Zonal-mean equations of motion*

Because the theory for eddy-forced zonal-mean flow has provided a formal framework for subsequent time-mean eddy forcing theories, the zonal-mean dynamics will be briefly reviewed. The zonal-averaging operator will be designated by brackets and the perturbation from the zonal-mean will be designated by asterisks. By assumption,

$$[*] = \frac{\partial}{\partial x}[\quad] = 0.$$

The $O(1)$ zonal-mean geostrophic and hydrostatic equations in dimensional units are

$$[u] = -\frac{1}{f_0 \rho_0} \frac{\partial}{\partial y}[P]$$

$$0 = -\frac{1}{\rho_0} \frac{\partial}{\partial z}[P] + g\alpha[\delta T].$$

Because $\partial/\partial x[P] = 0$, there can be no zonal-mean meridional geostrophic flow. Changes in $[u]$ are governed by the $O(\mathrm{Ro})$ equations of motion:

$$\frac{\partial}{\partial y}[v_a] = -\frac{\partial}{\partial z}[w] \tag{3}$$

$$\frac{\partial}{\partial t}[T] = -[w]\theta_z - \frac{\partial}{\partial y}[v^* T^*] \tag{4}$$

$$\frac{\partial}{\partial t}[u] = \beta y[v] + f_0[v_a] - \left[v^* \frac{\partial u^*}{\partial y}\right]. \tag{5}$$

While it is clear that the heat (4) and momentum (5) budgets are coupled, it is not intuitively obvious how the heat fluxes $[v^* T^*]$ accelerate or decelerate the mean zonal flow $[u]$. For this reason, it is often simpler to work with the potential vorticity budget, which combines (3)–(5) into a single equation:

$$\frac{\partial}{\partial t}[q] = -\frac{\partial}{\partial y}[v^* q^*] \tag{6}$$

$$q = f_0 + \beta y + \hat{\mathbf{z}} \cdot \nabla \times \mathbf{u} + f_0 \frac{\partial}{\partial z}\left(\frac{\delta T}{\theta_z}\right), \tag{7}$$

where the quasigeostrophic potential vorticity $q$ comprises the planetary vorticity $f = f_0 + \beta y$, the relative vorticity $\zeta = \hat{\mathbf{z}} \cdot \nabla \times \mathbf{u}$, and the stretching (thickness) vorticity

$$q_{st} = f_0 \frac{\partial}{\partial z}\left(\frac{\delta T}{\theta_z}\right).$$

By (6), heat and momentum fluxes that contribute to the meridional eddy potential vorticity flux will cause a temporal change in the zonal-mean potential vorticity $[q]$. Because changes in $[q]$ can be associated with changes in $[u]$, it can be expected that $[v^* q^*]$ can also force a temporal change in $[u]$.

Indeed, because the meridional eddy relative vorticity flux can be related to a meridional eddy advection of momentum: $[v^* \zeta^*] = -[v^* u_y^*]$ and the meridional eddy stretching flux can be related to a meridional eddy heat flux: $[v^* q_{st}^*] = f_0([v^* T^*]/\theta_z)_z$, a residual meridional–vertical circulation ($[\bar{v}]$, $[\bar{w}]$) can be introduced such that the only explicit eddy forcing in the zonal-mean momentum and heat equations appears as a meridional potential vorticity flux in the zonal-mean momentum equation:

$$[\tilde{v}] = [v_a] - \frac{\partial}{\partial z}\left(\frac{[v^* T^*]}{\theta_z}\right) \tag{8}$$

$$[\tilde{w}] = [w] + \frac{\partial}{\partial y}\left(\frac{[v^* T^*]}{\theta_z}\right) \tag{9}$$

$$\frac{\partial}{\partial y}[\tilde{v}] = -\frac{\partial}{\partial z}[\tilde{w}] \tag{10}$$

$$\frac{\partial}{\partial t}[T] = -[\tilde{w}]\theta_z \tag{11}$$

$$\frac{\partial}{\partial t}[u] = \beta y[v] + f_0[\tilde{v}_a] + [v^* q^*]. \tag{12}$$

Finally, with the eddy force on the zonal-mean flow, that is, the meridional eddy potential vorticity flux, expressed as the divergence of a meridional–vertical "Eliassen–Palm (EP) flux,"

$$\nabla\cdot\mathrm{EP} = [v^*q^*] \tag{13}$$

$$\mathrm{EP} = -[u^*v^*]\hat{y} + \frac{f_0}{\theta_z}[v^*T^*]\hat{z}, \tag{14}$$

the enstrophy equation can be put into the form of a wave activity equation (Andrews and McIntyre 1976)

$$\frac{\partial}{\partial t}\frac{[q^*q^*]}{2[q]_y} + \nabla\cdot\mathrm{EP} = \mathcal{D}, \tag{15}$$

where $\mathcal{D}$ is enstrophy dissipation, $[q]_y \neq 0$, and triple correlations and changes in the $[q]_y$ are assumed to be negligible. Thus, in the WKB limit of almost-plane waves on a slowly varying mean flow, the EP flux is not only a zonal momentum flux, but also is a wave activity flux and is proportional to the group velocity

$$\mathrm{EP} = \mathbf{c}\frac{[q^*q^*]}{2[q]_y}. \tag{16}$$

Equations (8)–(16) form the transformed Eulerian mean equations, commonly known as the Eliassen–Palm equations and have become widely used in the atmospheric literature (e.g., Simmons and Hoskins 1978; Edmon et al. 1980).

### b. *Time-mean equations of motion*

Because zonal averages are not always suitable, particularly for oceanic circulation, over the past 15 years there has been considerable effort in formulating an analogous eddy forcing theory for time-mean flow (Hoskins 1983; Hoskins et al. 1983; Trenberth 1986; Plumb 1986; Andrews 1990). The time-mean operator will be denoted by $\overline{(\ )}$ and the perturbation from the time-mean will be denoted by $(\ )'$. By assumption

$$\frac{\partial}{\partial t}\overline{(\ )} \sim \overline{(\ )'} \sim 0,$$

and by the QG approximation (1)–(2), $|\bar{\mathbf{u}}| \gg |\bar{\mathbf{U}}_a|$, $|\mathbf{u}'| \gg |\mathbf{U}_a'|$, and $|\theta_z| \gg |\overline{\delta T}_z|, |T_z'|$.

The $O(1)$ time-mean geostrophic and hydrostatic equations can be written in dimensional units as

$$f_0\hat{\mathbf{z}}\times\bar{\mathbf{u}} = -\frac{1}{\rho_0}\nabla\bar{P} \tag{17}$$

$$0 = -\frac{1}{\rho_0}\frac{\partial\bar{P}}{\partial z} + g\alpha\overline{\delta T}, \tag{18}$$

and the $O(\mathrm{Ro})$ time-mean continuity, heat, and momentum equations can be written as

$$\nabla\cdot\bar{\mathbf{u}}_a = -\frac{\partial\bar{w}}{\partial z} \tag{19}$$

$$\bar{\mathbf{u}}\cdot\nabla\overline{\delta T} = -\nabla\cdot\overline{\mathbf{u}'T'} - \bar{w}\theta_z \tag{20}$$

$$\bar{\mathbf{u}}\cdot\nabla\bar{\mathbf{u}} = -\beta y\hat{\mathbf{z}}\times\bar{\mathbf{u}} - f_0\hat{\mathbf{z}}\times\bar{\mathbf{u}}_a - \overline{\mathbf{u}'\cdot\nabla\mathbf{u}'}, \tag{21}$$

where $\mathbf{u}_a$ is the horizontal component of ageostrophic velocity $\mathbf{U}_a$. Note that we follow the meteorological convention (Gill 1982; Holton 1992) in which the pressure gradient appears only in the $O(1)$ equations.

The time-mean potential vorticity budget, which combines (19)–(21) into a single budget, can be written as

$$\bar{\mathbf{u}}\cdot\nabla\bar{q} = -\nabla\cdot\overline{\mathbf{u}'q'}.$$

The dynamics of the steady-state flow are inertial if the rhs is zero and eddy forced if the rhs is nonzero. A divergence in the eddy potential vorticity flux field can force the potential vorticity to change along mean streamlines, even for flow which conserves potential vorticity instantaneously.

Following the procedure used to derive the zonal-mean EP equations (8)–(15), Hoskins (1983) introduces a residual circulation such that the eddy force in the transformed time-mean momentum budget is in terms of potential vorticity fluxes: $\mathbf{F} = -\hat{\mathbf{z}}\times\overline{\mathbf{u}'q'} = \overline{v'q'}\hat{\mathbf{x}} - \overline{u'q'}\hat{\mathbf{y}}$. This force is similar in form to the eddy force in (12). However, while the zonally averaged meridional potential vorticity flux is divergent to within a uniform vector field, the time-mean potential vorticity flux can have a large rotational (nondivergent) component that has no affect upon the mean potential vorticity.

For this reason, Hoskins et al. (1983) explicitly remove a portion of the Hoskins (1983) eddy force that did not seem to match the changes in the mean flow. Assuming that $\partial/\partial y \gg \partial/\partial x$ and $\overline{v'v'} \gg \overline{u'u'}, \overline{u'v'}$, the resulting eddy force will be horizontally nondivergent. These conditions, however, are not met at the Gulf Stream 68°W study region (Cronin and Watts 1996). Using a less heuristic approach, Holopainen (1984) defines the nondivergent eddy force as $\mathbf{F}^{\mathrm{nondiv}} = -\hat{\mathbf{z}}\times\overline{\mathbf{u}'q'}^{\mathrm{div}}$ and estimates $\overline{\mathbf{u}'q'}^{\mathrm{div}}$ by solving the Poisson equation for its potential function.

The nondivergent/divergent decomposition is a difficult aspect of these time-mean eddy forcing theories. The mathematical decomposition used by Holopainen (1984) requires knowledge of the $\overline{\mathbf{u}'q'}^{\mathrm{div}}$ potential function's boundary conditions, and therefore has had limited use in oceanographic analyses. An alternative approach has been to determine analytical balances for the decompositions.

For conservative time-mean flow, Marshall and Shutts (1981) (MS) show that enstrophy contours can act as streamlines for a purely nondivergent component of the eddy potential vorticity flux

$$\overline{\mathbf{u}'q'}^{\mathrm{nondiv}} = \hat{\mathbf{z}}\times\nabla\frac{d\bar{\psi}}{d\bar{q}}\frac{\overline{q'^2}}{2}, \tag{22}$$

where $d\bar{\psi}/d\bar{q}$ is an empirically determined functional relationship between the mean streamlines and mean potential vorticity contours. A direct consequence of this definition is that the downgradient component of this nondivergent flux will balance the mean advection of enstrophy, and assuming that triple correlations can be neglected, the downgradient residual flux ($\overline{\mathbf{u}'q'}^* = \overline{\mathbf{u}'q'} - \overline{\mathbf{u}'q'}^{\text{nondiv}}$) will balance sources and sinks of enstrophy $\mathcal{D}$:

$$\bar{\mathbf{u}}\cdot\nabla\frac{\overline{q'q'}}{2} = -\overline{\mathbf{u}'q'}^{\text{nondiv}}\cdot\nabla\bar{q} \tag{23}$$

$$\frac{\partial}{\partial t}\frac{\overline{q'q'}}{2} + \overline{\mathbf{u}'q'}^*\cdot\nabla\bar{q} = \mathcal{D}. \tag{24}$$

While there is no guarantee that the residual MS flux is divergent, Plumb (1986) shows that the eddy force defined in terms of the residual: $\mathbf{F}^* = -\hat{\mathbf{z}}\times\overline{\mathbf{u}'q'}^*$ is consistent with the properties of a generalized Eliassen–Palm flux $M_T$. In particular, using (23) to estimate $\overline{\mathbf{u}'q'}^{\text{nondiv}}$ oriented along the mean gradient, the "pseudo-westward" eddy force can be estimated as

$$\mathbf{F}^*\cdot\hat{\mathbf{s}} = \overline{\mathbf{u}'q'}\cdot\nabla\bar{q}/|\nabla\bar{q}| + \bar{\mathbf{u}}\cdot\nabla\left(\frac{\overline{q'q'}}{2}\right)\Big/|\nabla\bar{q}|$$
$$= \nabla\cdot M_T, \tag{25}$$

where $\hat{\mathbf{s}} = \bar{q}/|\nabla\bar{q}|\times\hat{\mathbf{z}}$ is parallel to the potential vorticity (and mean streamline) contours. Thus, for small-amplitude QG eddies on a spatially slowly varying and nearly conservative time-mean flow, $M_T$ is the eddy flux of pseudo-westward momentum. The vector $\mathbf{M}_T$ is independent of the empirical factor $d\bar{\psi}/d\bar{q}$ and can be related to a wave activity flux even under nonconservative mean flow conditions

$$\frac{\partial}{\partial t}\frac{\overline{q'q'}}{2|\nabla\bar{q}|} + \nabla\cdot\mathbf{M}_T = \mathcal{D}. \tag{26}$$

For small amplitude, almost-plane waves on a slowly spatially varying time-mean field, the vector $\mathbf{M}_T$ will be parallel to the group velocity as in (16).

In regions where the enstrophy is homogeneous, advection of enstrophy is negligible and the vector $\mathbf{M}_T$ simplifies to $\mathbf{M}_R$, which does not depend upon the advection of enstrophy. Recently, Chester et al. (1994) evaluated Plumb's (1986) $\mathbf{M}_R$ in the recirculation region south of the Gulf Stream where the enstrophy gradient is negligible (i.e., where $\mathbf{M}_R \sim \mathbf{M}_T$) and found that the Gulf Stream is the source of eddy activity in the recirculation region. In the active Gulf Stream region it is doubtful that the simplified $\mathbf{M}_R$ can be used, since enstrophy advection is probably nonnegligible. However, with limited spatial resolution, which is typical of oceanic observation arrays, the enstrophy advection cannot be estimated and therefore $\nabla\cdot\mathbf{M}_T$ cannot be computed.

In the next section, a derivation of the time-mean eddy forcing is presented. As with the Hoskins et al. (1983) eddy force and the Holopainen (1984) eddy force, the theory relies upon the mathematical decomposition of the vector field. Divergent eddy thickness fluxes act as an eddy force on the mean flow as in Holopainen (1984). However, the barotropic eddy force is set as simply the eddy advection of momentum. The relation of this eddy force to divergent eddy potential vorticity fluxes is discussed.

## 3. Theory

### *a. The transformed Eulerian time-mean equations*

An advantage of using the transformed Eulerian mean equations is that the dynamical coupling between the heat and momentum equations are shown explicitly in the momentum equation as a form drag. That is, the horizontal ageostrophic flow is related to vertical motion through continuity, which in turn is related to heat fluxes:

$$\nabla\cdot\bar{\mathbf{u}}_a = -\frac{\partial\bar{w}}{\partial z}$$
$$= \frac{\partial}{\partial z}\left[\nabla\cdot\left(\frac{\overline{\mathbf{u}\delta T}}{\theta_z} + \frac{\overline{\mathbf{u}'T'}}{\theta_z}\right)\right]$$
$$= \nabla\cdot\frac{\partial}{\partial z}\left[\left(\frac{\overline{\mathbf{u}\delta T}}{\theta_z} + \frac{\overline{\mathbf{u}'T'}}{\theta_z}\right)\right]. \tag{27}$$

Note that the heat advection could be written in divergence form since $\bar{\mathbf{u}}$ and $\mathbf{u}'$ are horizontally nondivergent. By definition (2), $\theta_z$ is only a function of depth and therefore is unaffected by the horizontal divergence operator $\nabla = (\partial/\partial x, \partial/\partial y)$. Switching the order of differentiation, the divergent component of the ageostrophic velocity can be equated to the divergent component of the rhs of (27). Thus, with the nondivergent component expressed in terms of a streamfunction, $\bar{\mathbf{u}}_a^{\text{nondiv}} = -f_0^{-1}\hat{\mathbf{z}}\times\nabla\bar{\phi}_a$, the total (nondivergent + divergent) horizontal mean ageostrophic flow field can be written as

$$\bar{\mathbf{u}}_a = -\frac{1}{f_0}\hat{\mathbf{z}}\times\nabla\bar{\phi}_a + \left[\frac{\partial}{\partial z}\left(\frac{\bar{\mathbf{u}}\,\bar{T}}{\theta_z}\right)\right]^{\text{div}} + \left[\frac{\partial}{\partial z}\left(\frac{\overline{\mathbf{u}'T'}}{\theta_z}\right)\right]^{\text{div}} \tag{28}$$

or equivalently as

$$\bar{\mathbf{u}}_a = \tilde{\mathbf{u}}_a + \left[\frac{\partial}{\partial z}(\overline{\mathbf{u}'T'}/\theta_z)\right]^{\text{div}},$$

where $\tilde{\mathbf{u}}_a$ is the residual horizontal mean ageostrophic flow.

This form of the ageostrophic velocity (28) explicitly shows the dynamically important coupling of the mean heat and momentum equations. Eddy heat fluxes enter the mean momentum budget through the Coriolis

torque on the ageostrophic flow. With the simplifying assumption that (28) can be written in terms of divergent heat fluxes, the thermal eddy force can be expressed as

$$\mathbf{F}_{\text{therm}} = -f_0\hat{z}\times\left[\frac{\partial}{\partial z}\left(\frac{\overline{\mathbf{u}'T'}}{\theta_z}\right)\right]^{\text{div}} \sim -f_0\hat{\mathbf{z}}\times\frac{\partial}{\partial z}\left(\frac{\overline{\mathbf{u}'T'}^{\text{div}}}{\theta_z}\right) = \frac{\partial}{\partial z}\left(\frac{f_0}{\theta_z}\overline{v'T'}^{\text{div}}\right)\hat{\mathbf{x}} - \frac{\partial}{\partial z}\left(\frac{f_0}{\theta_z}\overline{u'T'}^{\text{div}}\right)\hat{\mathbf{y}}. \tag{29}$$

For reasons that will be discussed in the section 3b, the barotropic component of the eddy force will be set as the eddy advection of momentum

$$\mathbf{F}_{\text{mom}} = -\overline{\mathbf{u}'\cdot\nabla\mathbf{u}'} = -\left(\frac{\partial}{\partial x}\overline{u'u'} + \frac{\partial}{\partial y}\overline{u'v'}\right)\hat{\mathbf{x}} - \left(\frac{\partial}{\partial x}\overline{u'v'} + \frac{\partial}{\partial y}\overline{v'v'}\right)\hat{\mathbf{y}}. \tag{30}$$

Grouping the thermal eddy forcing with the eddy advection of momentum, the net eddy forcing can be expressed in terms of a three-dimensional divergence of an eddy stress tensor $\mathbf{E}$:

$$\mathbf{F}_{\text{therm}} + \mathbf{F}_{\text{mom}} = \nabla_3\cdot\mathbf{E}, \tag{31}$$

where $\nabla_3 = (\partial/\partial x, \partial/\partial y, \partial/\partial z)$ and

$$\mathbf{E} = \begin{pmatrix} -\overline{u'u'} & -\overline{u'v'} & \frac{f_0}{\theta_z}\overline{v'T'}^{\text{div}} \\ -\overline{u'v'} & -\overline{v'v'} & -\frac{f_0}{\theta_z}\overline{u'T'}^{\text{div}} \\ \frac{f_0}{\theta_z}\overline{v'T'}^{\text{div}} & -\frac{f_0}{\theta_z}\overline{u'T'}^{\text{div}} & * \end{pmatrix}. \tag{32}$$

Although the eddy force vector $\nabla_3\cdot\mathbf{E}$ technically is three-dimensional, its vertical component is undefined since the geostrophic flow does not have a vertical component.

As one might perhaps expect, the residual horizontal ageostrophic mean flow $\tilde{\mathbf{u}}_a$ is, in fact, part of a three-dimensional residual circulation $(\tilde{u}_a, \tilde{v}_a, \tilde{w})$, where $\tilde{w}$ transforms the mean heat equation

$$\tilde{\mathbf{u}}_a = \bar{\mathbf{u}}_a - \frac{\partial}{\partial z}\left(\frac{\overline{\mathbf{u}'T'}^{\text{div}}}{\theta_z}\right). \tag{33}$$

$$\tilde{w} = \bar{w} + \nabla\cdot\left(\frac{\overline{\mathbf{u}'T'}^{\text{div}}}{\theta_z}\right) \tag{34}$$

$$\nabla\cdot\tilde{\mathbf{u}}_a = -\frac{\partial\tilde{w}}{\partial z} \tag{35}$$

$$\bar{\mathbf{u}}\cdot\nabla\bar{T} + \tilde{w}\theta_z = 0 \tag{36}$$

$$\bar{\mathbf{u}}\cdot\nabla\bar{\mathbf{u}} = -\beta y\hat{\mathbf{z}}\times\bar{\mathbf{u}} - f_0\hat{\mathbf{z}}\times\tilde{\mathbf{u}}_a + \nabla_3\cdot\mathbf{E}. \tag{37}$$

Because $\mathbf{F}_{\text{mom}}$ is the eddy advection of momentum, the barotropic portion of the transformed time-mean momentum budget (37) is identical to the traditional formulation (21). The crucial difference between this formulation and the traditional formulation (21) is that the dynamical coupling between the heat and momentum budgets is explicit in the momentum budget. All the dynamical eddy fluxes appear explicitly exclusively in the transformed momentum budget (37) in terms of a divergence of an eddy stress tensor. Thus, (32)–(37) represent the transformed Eulerian time-mean equations.

### *b. Divergent eddy potential vorticity fluxes*

A key element of the Eliassen–Palm equations is relating the eddy force $\mathbf{F}_{\text{therm}} + \mathbf{F}_{\text{mom}} = \nabla\cdot\mathbf{E}$ to eddy potential vorticity fluxes. Recall that the eddy potential vorticity flux comprises a relative vorticity flux $\overline{\mathbf{u}'\zeta'} = \overline{\mathbf{u}'(\hat{\mathbf{z}}\cdot\nabla\times\mathbf{u}')}$ and a stretching (thickness) flux $\overline{\mathbf{u}'q'_{st}} = \overline{\mathbf{u}'f_0(\partial/\partial z)(T'/\theta_z)}$.

Using the thermal wind relation to write the vertical shear in terms of horizontal temperature gradients, $\mathbf{F}_{\text{therm}}$ can be related to divergent eddy stretching fluxes:

$$\mathbf{F}_{\text{therm}} = -f_0\hat{\mathbf{z}}\times\left[\frac{\partial}{\partial z}\left(\frac{\overline{\mathbf{u}'T'}}{\theta_z}\right)\right]^{\text{div}} = -f_0\hat{\mathbf{z}}\times\left[\overline{\mathbf{u}'\frac{\partial}{\partial z}\left(\frac{T'}{\theta_z}\right)} - \hat{\mathbf{z}}\times\nabla\frac{g\alpha}{2\theta_z}\overline{T'^2}\right]^{\text{div}}, = -\hat{\mathbf{z}}\times\overline{\mathbf{u}'q'_{st}}^{\text{div}}$$

where

$$\left(\hat{\mathbf{z}}\times\nabla\frac{g\alpha}{2\theta_z}\overline{T'^2}\right)^{\text{div}} = 0$$

since any vector field in the form $\hat{\mathbf{z}}\times\nabla\phi$ is guaranteed to be nondivergent. Likewise, using the vector identity

$$(A\cdot\nabla)B = \nabla(A\cdot B) - A\times(\nabla\times B) - B\times(\nabla\times A) - (B\cdot\nabla)A,$$

$\mathbf{F}_{\text{mom}}$ can be related to relative vorticity fluxes:

$$\mathbf{F}_{\text{mom}} = -\overline{(\mathbf{u}'\cdot\nabla)\mathbf{u}'} = -\overline{(\nabla\times\mathbf{u}')\times\mathbf{u}'} - \nabla\left(\frac{\overline{\mathbf{u}'\cdot\mathbf{u}'}}{2}\right) = -\hat{\mathbf{z}}\times\overline{\mathbf{u}'\zeta'}^{\text{div}} - \hat{\mathbf{z}}\times\overline{\mathbf{u}'\zeta'}^{\text{nondiv}} - \nabla\text{EKE},$$

where $\text{EKE} = (\overline{\mathbf{u}'\cdot\mathbf{u}'})/2$ is the eddy kinetic energy.

In general, a vector can have a uniform component, a purely divergent component, a purely rotational component, and a purely deformational component (Bluestein 1992). If $\overline{\mathbf{u}'q'}^{\text{div}}$ is purely divergent, then $-\hat{\mathbf{z}} \times \overline{\mathbf{u}'q'}^{\text{div}}$ is purely rotational; $-\hat{\mathbf{z}} \times \overline{\mathbf{u}'q'}^{\text{nondiv}}$ can be expressed as the gradient of a potential function and therefore is irrotational: $-\hat{\mathbf{z}} \times \overline{\mathbf{u}'q'}^{\text{nondiv}} = -\hat{\mathbf{z}} \times (\hat{\mathbf{z}} \times \nabla\psi_q) = \nabla\psi_q$. The eddy force $\mathbf{F}_{\text{eddy}} = \mathbf{F}_{\text{therm}} + \mathbf{F}_{\text{mom}} = \nabla \cdot \mathbf{E}$ can therefore be decomposed into rotational and irrotational components

$$\mathbf{F}^{\text{rot}}_{\text{eddy}} = \mathbf{F}_{\text{therm}} + \mathbf{F}^{\text{rot}}_{\text{mom}} = -\hat{\mathbf{z}} \times \overline{\mathbf{u}'q'}^{\text{div}} \quad (38)$$

$$\mathbf{F}^{\text{irrot}}_{\text{eddy}} = \mathbf{F}^{\text{irrot}}_{\text{mom}} = -\hat{\mathbf{z}} \times \overline{\mathbf{u}'\zeta'}^{\text{nondiv}} - \nabla\text{EKE}. \quad (39)$$

A divergent eddy potential vorticity flux acts as a rotational eddy force and will tend to induce vorticity in the time-mean geostrophic flow. If the irrotational eddy force is divergent, then the eddy force enters the balanced divergence equation. However, if the irrotational eddy force is nondivergent, the eddy force will tend to induce deformation (e.g., confluence and diffluence) in the mean flow. The irrotational eddy force can be dynamically important and therefore is included in the eddy force.

### c. *Eddy forcing mechanism*

To gain intuition into the eddy forcing mechanism, it is helpful to view the mean momentum equation in natural coordinates. Letting $\hat{\mathbf{s}}$ be the direction defined by the downstream mean geostrophic flow, and $\hat{\mathbf{n}}$ be the direction normal and to the left of $\hat{\mathbf{s}}$ ($\hat{\mathbf{s}} \times \hat{\mathbf{n}} = \hat{\mathbf{z}}$), the $\hat{\mathbf{s}}$ and $\hat{\mathbf{n}}$ components of the mean momentum budget (37) can be written in natural coordinates relative to the time-mean flow as

$$|\bar{\mathbf{u}}| \frac{\partial|\bar{\mathbf{u}}|}{\partial s} = f_0\hat{\mathbf{n}}\cdot\tilde{\mathbf{u}}_a + \hat{\mathbf{n}}\cdot\overline{\mathbf{u}'q'_{st}}^{\text{div}} + \hat{\mathbf{n}}\cdot\overline{\mathbf{u}'\zeta'} - \frac{\partial\text{EKE}}{\partial s} \quad (40)$$

$$\frac{|\bar{\mathbf{u}}|^2}{R} = -\beta y|\bar{\mathbf{u}}| - f_0\hat{\mathbf{s}}\cdot\tilde{\mathbf{u}}_a - \hat{\mathbf{s}}\cdot\overline{\mathbf{u}'q'_{st}}^{\text{div}} - \hat{\mathbf{s}}\cdot\overline{\mathbf{u}'\zeta'} - \frac{\partial\text{EKE}}{\partial n}. \quad (41)$$

Here $|\bar{\mathbf{u}}| = \hat{\mathbf{s}}\cdot\bar{\mathbf{u}}$ is the speed of the time-mean flow, and $R$ is the radius of curvature of the mean streamlines with positive values corresponding to cyclonic curvature.

Consider the forcing due to the gradient in the eddy kinetic energy. If the eddy kinetic energy increases along mean streamlines, then by (40) there will be a tendency for the speed (and thus also the kinetic energy) of the mean flow to decrease. This eddy force therefore implies a conversion of mean kinetic energy to eddy kinetic energy. The relation of the eddy stress tensor to the mean to eddy energy conversion rates is discussed further in the section 3e.

Now consider the forcing due to the relative vorticity flux. As illustrated in Fig. 1, for an eastward mean jet, a northward flux of anticyclonic vorticity and/or a southward flux of cyclonic vorticity will tend to decelerate the mean eastward flow. Likewise, an eastward cyclonic flux will tend to turn the mean eastward flow southward and thus introduce an anticyclonic curvature to the mean flow. Because the nondivergent relative vorticity fluxes do not affect the vorticity of the mean flow, the mean curvature vorticity induced by the nondivergent relative vorticity flux will be balanced by a reduction in the mean shear vorticity.

The forcing due to the divergent eddy stretching fluxes is also illustrated in Fig. 1. A cross-stream stretching "thickness" flux will tend to make the thermocline less steep, and thus by thermal wind, will tend to make the flow more barotropic (less vertically sheared) by decelerating the upper-level flow and accelerating the deep-level flow. Similarly, a stretching flux oriented to make the thermocline shallower downstream will cause the vertically sheared flow to turn to the right (e.g., turn the eastward flow southward) in the Northern Hemisphere. Momentum and thermal eddy forces can also be thought of as viscouslike forces: The eddy advection of momentum redistributes the momentum horizontally, while divergent stretching fluxes redistribute the momentum vertically. The divergent stretching flux eddy force can thus be interpreted as an interfacial form drag.

In summary, the $\mathbf{F}_{\text{therm}}$ and $\mathbf{F}_{\text{mom}}$ vectors can be superimposed on plots of the mean streamlines of flow to visually determine how the eddies might be responsible for the change in speed and direction of the time-mean flow. Where the eddy force is oriented downstream, the eddies tend to accelerates the flow; where the force is oriented normal and to the left of the mean streamlines, the eddies tend to cause the mean flow to change direction by inducing cyclonic curvature. If the pattern of the eddy force is rotational, the eddy force will tend to induce vorticity in the mean flow. If the $\mathbf{F}_{\text{mom}}$ pattern is irrotational and nondivergent, the eddy force will tend to induce deformation in the mean flow.

### d. *The wave activity flux*

To interpret the eddy stress tensor $\mathbf{E}$ in terms of a wave activity flux for small amplitude almost-plane waves on a slow spatially varying background field (WKB limit), the eddy forcing must be equivalent to a downgradient potential vorticity flux, such as in the zonal-mean formulism (13)–(16) or Plumb's (1986) elegant relationship between $\mathbf{M}_T$ and the group velocity (25)–(26). By inspection of (38)–(39), this is only possible under certain conditions, for example, that 1) the eddy force is oriented along mean potential vorticity contours $\bar{q}$ with high values to the left, 2) the stretching potential vorticity flux field is purely divergent, and 3) the eddy kinetic energy does not vary

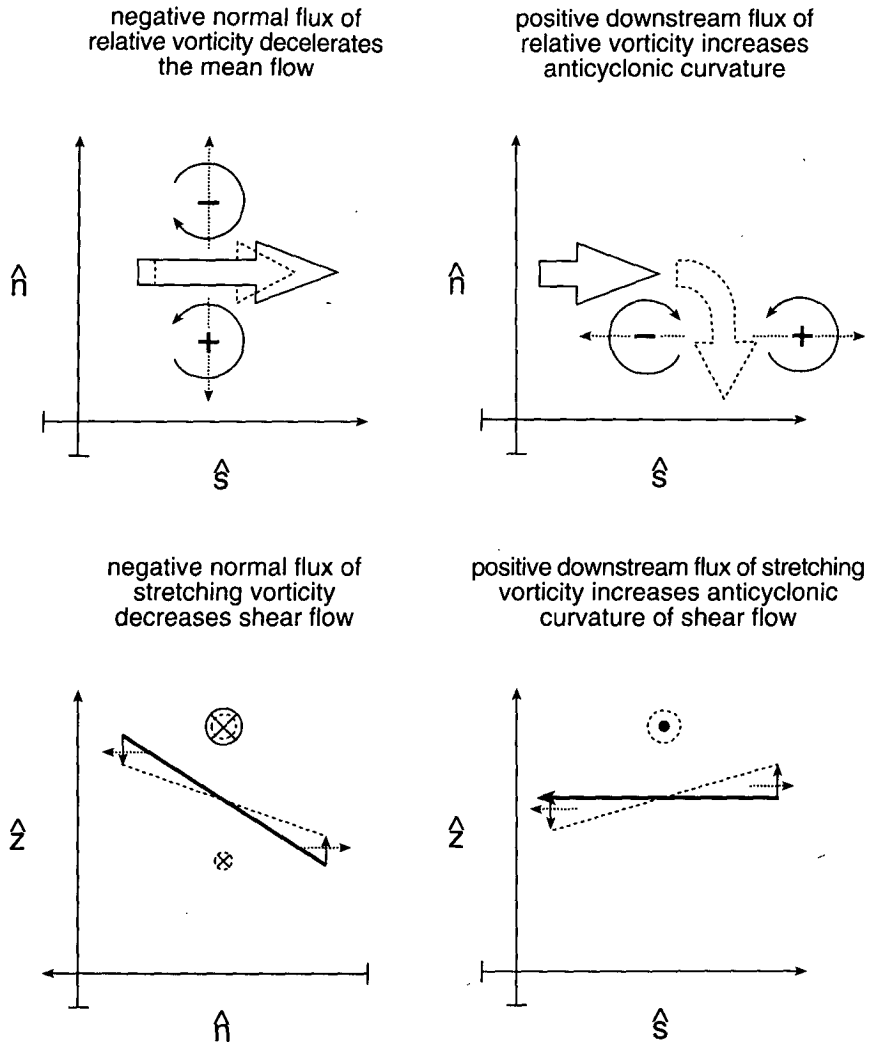


FIG. 1. A schematic showing the effect (dashed line) of the downstream and normal components of the eddy vorticity and eddy stretching fluxes (dotted line) on the time-mean flow.

along $\bar{q}$ contours. While these conditions appear to be quite restrictive, they in fact are characteristic of zonally averaged fields with reentrant boundary conditions. Under these conditions $\nabla_3 \cdot \mathbf{E}$ will act as a wave activity flux and if the enstrophy does not vary along mean streamlines, the component of $\mathbf{E}$ oriented along mean potential vorticity contours will be proportional to the group velocity as in (16).

*e. Eddy-mean energy conversion*

In the previous sections, it was shown that eddies can cause the mean flow to evolve along mean streamlines. To form a complete eddy–mean flow interaction analysis one must also look at how instabilities in the mean flow can generate eddies. In this section, it is shown that part of the net work done by the eddy stress tensor is the conversion of mean energy to eddy energy.

Because only the divergent heat fluxes are related to heat advection and baroclinic conversion events, Cronin and Watts (1996) define the rate of baroclinic conversion of mean potential energy to eddy potential energy to be the downgradient *divergent* eddy heat flux. With the barotropic conversion of mean kinetic energy to eddy kinetic energy defined as the traditional downgradient momentum flux, the rate of conversion of mean to eddy energy is then

$$\text{energy conversion rate} = -\frac{g\alpha}{\theta_z}\overline{\mathbf{u}'T'}^{\text{div}} \cdot \nabla\bar{T} - \overline{u'u'}\frac{\partial \bar{u}}{\partial x} - \overline{u'v'}\left(\frac{\partial \bar{u}}{\partial y} + \frac{\partial \bar{v}}{\partial x}\right) - \overline{v'v'}\frac{\partial \bar{v}}{\partial y}. \quad (42)$$

The essential physics of this conversion rate is contained within the physics of the eddy stress tensor. As shown in standard fluid mechanics texts [e.g., White (1974, p. 74), the net rate of work done by the viscous stress $\mathbf{T}$ is $\nabla\cdot(\mathbf{u}\cdot\mathbf{T})$ and is composed of two parts:

$$\nabla\cdot(\mathbf{u}\cdot\mathbf{T}) = \mathbf{u}\cdot(\nabla\cdot\mathbf{T}) + T_{ij}\frac{\partial}{\partial x_j}u_i, \qquad (43)$$

where indicial notation with summation over repeated indices (indices $i, j$ can be 1, 2, or 3 corresponding to the Cartesian directions east, north, and up) is used to clarify the vector and tensor multiplications in the second term on the rhs.

The first term on the rhs of (43), $\mathbf{u}\cdot(\nabla\cdot\mathbf{T})$, is the rate of work done by the viscous force to change the speed (i.e., kinetic energy) of the flow. The budget for the kinetic energy of the mean flow can be derived by taking the scalar product of the mean flow $\bar{\mathbf{u}}$ and the mean momentum equation (21). Note that $\bar{\mathbf{u}}\cdot(\bar{\mathbf{u}}\cdot\nabla\bar{\mathbf{u}}) = \bar{\mathbf{u}}\cdot\nabla\mathrm{MKE}$ where $\mathrm{MKE} = \frac{1}{2}\bar{\mathbf{u}}\cdot\bar{\mathbf{u}}$ and that the geostrophic relation (17) can be used to write the rate of work, done by the residual ageostrophic flow torque as a rate of mean pressure work: $\bar{\mathbf{u}}\cdot(-f_0\hat{\mathbf{z}}\times\tilde{\mathbf{u}}_a) = -\tilde{\mathbf{u}}_a\cdot\nabla\bar{P}/\rho_0$. Thus, the MKE budget can be written as

$$\bar{\mathbf{u}}\cdot\nabla\mathrm{MKE} = -\tilde{\mathbf{u}}_a\cdot\nabla\frac{\bar{P}}{\rho_0} + \underbrace{\bar{\mathbf{u}}\cdot(\nabla\cdot\mathbf{E})}_{W_{\mathrm{eddy}}}, \qquad (44)$$

where $\bar{\mathbf{u}}\cdot(\nabla\cdot\mathbf{E}) = W_{\mathrm{eddy}}$ is the rate of work done by the eddy stresses to change the speed of the mean geostrophic flow.

The second term on the rhs of (43)

$$T_{ij}\frac{\partial}{\partial x_j}u_i$$

is the rate of increase in the internal energy due to the action of the viscous stress. Because the stress tensor is symmetric, this second term reduces to the scalar product of the stress tensor $\mathbf{T}$ and the strain rate tensor $\mathbf{S}$. The time-mean geostrophic strain rate tensor is

$$\mathbf{S} = \begin{pmatrix} \dfrac{\partial\bar{u}}{\partial x} & \dfrac{1}{2}\left(\dfrac{\partial\bar{v}}{\partial x}+\dfrac{\partial\bar{u}}{\partial y}\right) & \dfrac{1}{2}\left(0+\dfrac{\partial\bar{u}}{\partial z}\right) \\ \dfrac{1}{2}\left(\dfrac{\partial\bar{v}}{\partial x}+\dfrac{\partial\bar{u}}{\partial y}\right) & \dfrac{\partial\bar{v}}{\partial y} & \dfrac{1}{2}\left(0+\dfrac{\partial\bar{v}}{\partial z}\right) \\ \dfrac{1}{2}\left(0+\dfrac{\partial\bar{u}}{\partial z}\right) & \dfrac{1}{2}\left(0+\dfrac{\partial\bar{v}}{\partial z}\right) & 0 \end{pmatrix},$$

and the scalar product of the eddy stress tensor $\mathbf{E}$ given by (32) and the mean strain rate tensor is

$$\mathbf{E}\cdot\mathbf{S} = -\overline{u'u'}\frac{\partial\bar{u}}{\partial x} - \overline{u'v'}\left(\frac{\partial\bar{u}}{\partial y}+\frac{\partial\bar{v}}{\partial x}\right) - \overline{v'v'}\frac{\partial\bar{v}}{\partial y} + \frac{f_0}{\theta_z}\overline{v'T'}^{\mathrm{div}}\frac{\partial\bar{u}}{\partial z} - \frac{f_0}{\theta_z}\overline{u'T'}^{\mathrm{div}}\frac{\partial\bar{v}}{\partial z}.$$

By thermal wind, the vertical shear in the mean velocity can be related to the horizontal mean temperature gradient and

$$\mathbf{E}\cdot\mathbf{S} = -\overline{u'u'}\frac{\partial\bar{u}}{\partial x} - \overline{u'v'}\left(\frac{\partial\bar{u}}{\partial y}+\frac{\partial\bar{v}}{\partial x}\right) - \overline{v'v'}\frac{\partial\bar{v}}{\partial y} - \frac{g\alpha}{\theta_z}\overline{\mathbf{u}'T'}^{\mathrm{div}}\cdot\nabla\bar{T}.$$

Therefore, $\mathbf{E}\cdot\mathbf{S}$ is the rate of conversion from mean to eddy energy (42) in the eddy energy budget as defined by Cronin and Watts (1996). The net rate of work done by the eddy stresses $\mathbf{E}$ is the combined rate of work done to change the kinetic energy of the mean flow and the rate of conversion from mean energy to eddy energy.

In section 3a it was shown that the three-dimensional divergence of the eddy stress tensor $\nabla_3\cdot\mathbf{E}$ is a source of mean momentum. In section 3d it was shown that under certain circumstances the eddy stress tensor when aligned with the mean potential vorticity contours could be interpreted in terms of a wave activity flux. From the discussion presented here, the eddy stress tensor can also be associated with sources of eddy energy when the eddy stresses are aligned with the strain rate of the mean flow. The eddy forcing and eddy energetics diagnostics presented here and in Cronin and Watts (1996) thus form complementary analyses of the eddy–mean flow interaction.

## 4. Data

For two years, from June 1988 to August 1990, twelve moorings arranged along three lines measured

temperature and velocity at levels 400 m, 700 m, 1000 m, and 3500 m (Shay et al. 1994). The array, shown in Fig. 2, was centered at 68°W with two of the three lines transecting the full Eulerian mean field. Additionally, inverted echo sounders (IESs) were set around the periphery of the mooring array and with pressure sensors at the base of each mooring (Tracey and Watts 1991). IESs are acoustic bottom moored instruments used to determine the depth of the 12°C isotherm, that is, the depth of the main thermocline. As discussed in Cronin and Watts (1996, hereinafter called Part I), the IESs could also be used to determine the temperature at any depth within the thermocline, including 400, 700, and 1000 m. The temperature array is thus as large as the combined IES and current meter array. The mooring and IES spacing, 56 km in cross stream and 65 km in downstream, is less than the Gulf Stream path's correlation length scale; therefore, the array resolves the mesoscale eddy structure. Subinertial and tidal fluctuations were removed by applying a 40-h low-pass filter to all measurements.

The upper three level temperature and velocity mooring measurements were interpolated (and extrapolated) to constant depths of 400, 700, and 1000 m using Hogg's (1991) mooring motion correction scheme. Details of this procedure as applied to this dataset can be found in Part I and in Cronin et al. (1992). The constant horizon temperature and velocity measurements at all four levels were then mapped onto a horizontal grid with 10-km spacing using optimal interpolation (Bretherton et al. 1976). It should be noted, however, that we use a spacing of $2\Delta x$, $2\Delta y = 40$ km in our centered finite difference approximation of the horizontal gradient operator.

As discussed in Part I, because the velocity fields at and below 400 m are expected to be nearly geostrophic, a nondivergent vector optimal interpolation has been used to map the velocity field. The mapped velocity fields are therefore associated with a streamfunction $\psi$ ($\mathbf{u} = \hat{\mathbf{z}} \times \nabla\psi$) and are assumed to satisfy the geostrophic relation (1). The mapped velocities and streamlines are therefore consistent with the quasigeostrophic assumptions of the preceding sections.

The OI analysis also produces error maps as a function of the input variables (e.g., if pressure as well as velocity is used to estimate the geostrophic velocity field), the instrument spacing, the correlation length scale, and the measurement and ageostrophic noise of the input fields. Using the methodology described in appendix B of Part I, the OI error fields are used to compute the measurement errors for the budgets. These error fields reflect the array's ability to interpolate and extrapolate the measurements horizontally and create a field that can be mapped, rather than the statistical error field. Nevertheless, we believe that the 26-month time-averaged fields might represent the long-term mean fields. During the 26-month record, six large amplitude trough events formed locally and a trough feature is

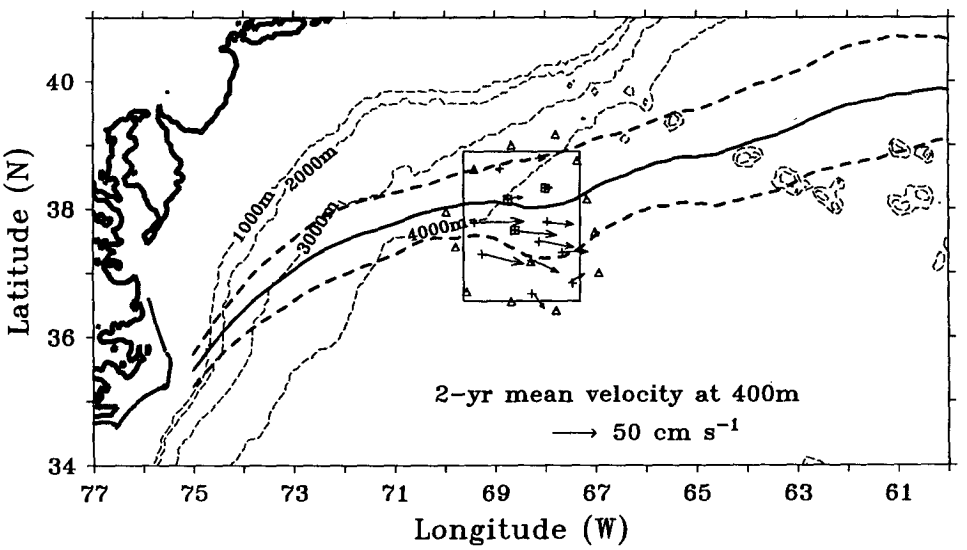


FIG. 2. The boxed study region shows the area in which the measured fields are mapped. Plus marks indicate mooring sites. Triangles indicate inverted echo sounder sites used to estimate temperature at 400, 700, and 1000 m. Squares indicate moorings with an additional upward looking ADCP. The mean Gulf Stream path (thick solid line) and the ±1 standard deviation envelope (thick dashed lines) are computed from 93 months of satellite IR images (Lee 1994). Twelve moorings were in place during the first deployment year. During the second deployment year a thirteenth mooring between the second and third lines was set in place; however, two critical instruments on the secondmost southern mooring along the second line failed during the second year. Thus although 13 moorings are shown, only 12 obtained useful data for each of the two years.

evident in the upper level 26-month averaged fields. A similar trough feature is also evident in the 93-month average satellite IR SST field (Lee 1994). Thus, the steady-state eddy forcing theory developed in the preceding section will be applied to this dataset.

## 5. Analysis

### a. *Estimating the eddy forces at 68°W*

In order to visualize the effect of the eddy forces, the eddy force vectors are superimposed upon the mean streamlines. The alongstream component of the eddy force changes the speed of the mean flow and is most easily analyzed by evaluating the mean kinetic energy (MKE) budget (44). The rate of work done by the thermal force to change the speed of the mean flow is $W_{\text{therm}} = \bar{\mathbf{u}} \cdot \mathbf{F}_{\text{therm}}$ and the rate of work done by the eddy momentum flux forcing is $W_{\text{mom}} = \bar{\mathbf{u}} \cdot \mathbf{F}_{\text{mom}}$.

Because the OI procedure has interpolated the data onto a regular grid at each level, the horizontal derivatives in $\mathbf{F}_{\text{mom}}$ (30) can be approximated by a horizontal centered finite difference operator with $2\Delta x$, $2\Delta y$ = 40 km. On the other hand, because the array has instrumentation only at 400, 700, 1000, and 3500 m, a vertical centered finite difference operator (with $2\Delta z$ = 600 m) can be used only at the 700-m level. However, if it is assumed that the ocean behaves as a two-layer fluid, with heat fluxes occurring only at the thermocline (~700 m), then a two-layer upper and deep level $\mathbf{F}_{\text{therm}}$, can be estimated as

$$\mathbf{F}_{\text{therm}|\text{upper}} = -\frac{f_0}{\theta_z H_1}\overline{v'T'}^{\text{div}}|_{700\text{ m}}\hat{\mathbf{x}} + \frac{f_0}{\theta_z H_1}\overline{u'T'}^{\text{div}}|_{700\text{ m}}\hat{\mathbf{y}} \quad (45)$$

$$\mathbf{F}_{\text{therm}|\text{deep}} = \frac{f_0}{\theta_z H_2}\overline{v'T'}^{\text{div}}|_{700\text{ m}}\hat{\mathbf{x}} + \frac{f_0}{\theta_z H_2}\overline{u'T'}^{\text{div}}|_{700\text{ m}}\hat{\mathbf{y}}, \quad (46)$$

where $H_1 \sim 700$ m and $H_2 \sim 4000$ m. Because the temperature front is well defined throughout the upper layer and is weak near the bottom (Watts 1983; Hall and Fofonoff 1993), the heat fluxes will be large throughout the upper layer and negligible near the bottom. Thus, it is expected that the two-layer approximation of $\mathbf{F}_{\text{therm}}$ (45)–(46) produces a good estimate of $\mathbf{F}_{\text{therm}|\text{deep}}$ and a poor estimate of $\mathbf{F}_{\text{therm}|\text{upper}}$. Further caution is warranted in using the two-layer thermal forcing since in a centered finite difference sense $\mathbf{F}_{\text{therm}|\text{upper}}$ and $\mathbf{F}_{\text{therm}|\text{deep}}$ are nominally at depths of 350 and 2700 m, which are slightly higher in the water column than 400 and 3500 m. Nevertheless, it is instructive to see the patterns of these force vectors in relation to $\mathbf{F}_{\text{mom}}$ and the mean streamlines.

As in Part I, the mean and eddy fields are defined to be respectively the 26-month time-averaged field and the perturbation from this mean. Likewise, we let $\theta_z$ be a function of depth equal to 1°C per 60 m ($1.7 \times 10^{-4}$°C cm$^{-1}$) for the 400- and 700-m levels, 1°C per 100 m ($1.0 \times 10^{-4}$°C cm$^{-1}$) for the 1000-m level, and 1°C per 1000 m ($1.0 \times 10^{-5}$°C cm$^{-1}$) for the deep level. A value of $8.9 \times 10^{-5}$ s$^{-1}$ was used for the Coriolis parameter $f_0$ and a value of $1.8 \times 10^{-13}$ cm$^{-1}$ s$^{-1}$ was used for $\beta$ corresponding to a central latitude of 37.6°N (−40 km in the coordinate system used in Figs. 3–8).

The most difficult part of the analysis is evaluating the divergent heat fluxes. In practice, it is nearly impossible to evaluate the purely divergent component of a vector field. With open boundary conditions, the Poisson method cannot be used to determine the irrotational flux. Instead the "divergent" heat flux will be estimated using the Marshall and Shutts (1981) method. The term divergent is placed in quotes here because the method defines a nondivergent flux, the residual of which is not guaranteed to be purely divergent. Briefly, assuming that mean temperature contours are nearly parallel to mean streamlines, the empirically determined factor $d\bar{\psi}/d\bar{T}$ can be used to define a purely nondivergent heat flux in terms of temperature variance. The divergent heat flux is estimated as the residual

$$\overline{\mathbf{u}'T'}^{\text{nondiv}} = \hat{\mathbf{z}} \times \nabla \frac{d\bar{\psi}}{d\bar{T}} \frac{1}{2}\overline{T'^2} \quad (47)$$

$$\overline{\mathbf{u}'T'}^{\text{"div"}} = \overline{\mathbf{u}'T'} - \overline{\mathbf{u}'T'}^{\text{nondiv}}. \quad (48)$$

As shown by MS, the residual downgradient heat flux will be balanced by an upgradient vertical heat flux and therefore implies a conversion of mean potential energy to eddy kinetic energy. Nevertheless, while $\overline{\mathbf{u}'T'}^{\text{nondiv}}$ is purely horizontally nondivergent, the residual (48) will not necessarily be purely horizontally divergent. Leakage of nondivergent heat fluxes into the "divergent" heat flux component will add and subtract a vector field to respectively $\mathbf{F}_{\text{therm}}$ (29) and the Coriolis torque on the residual ageostrophic flow (33).

As shown in Fig. 3, the conversion factor $d\bar{\psi}/d\bar{T}$ for each level was estimated by fitting a line to the mean streamline and temperature data, which were from the low-error (unshaded) region of the maps. Marshall and Shutts (1981) recommend that this method be used only in regions where the mean flow conserves heat. This requirement is not strictly satisfied at 68°W. The $\bar{\psi}$ and $\bar{T}$ maps in Fig. 3a feature a trough in the southern portion of the 400–1000-m level maps and a permanent cyclone in the deep layer. At 1000 m, the trough in the mean temperature field lags the trough in the mean streamlines. Nevertheless, as can be seen in Fig. 3b, the functional relation between $\bar{T}$ and $\bar{\psi}$ is to a good approximation linear, and the relation did not change substantially when smaller subregions were used to evaluate the relation.

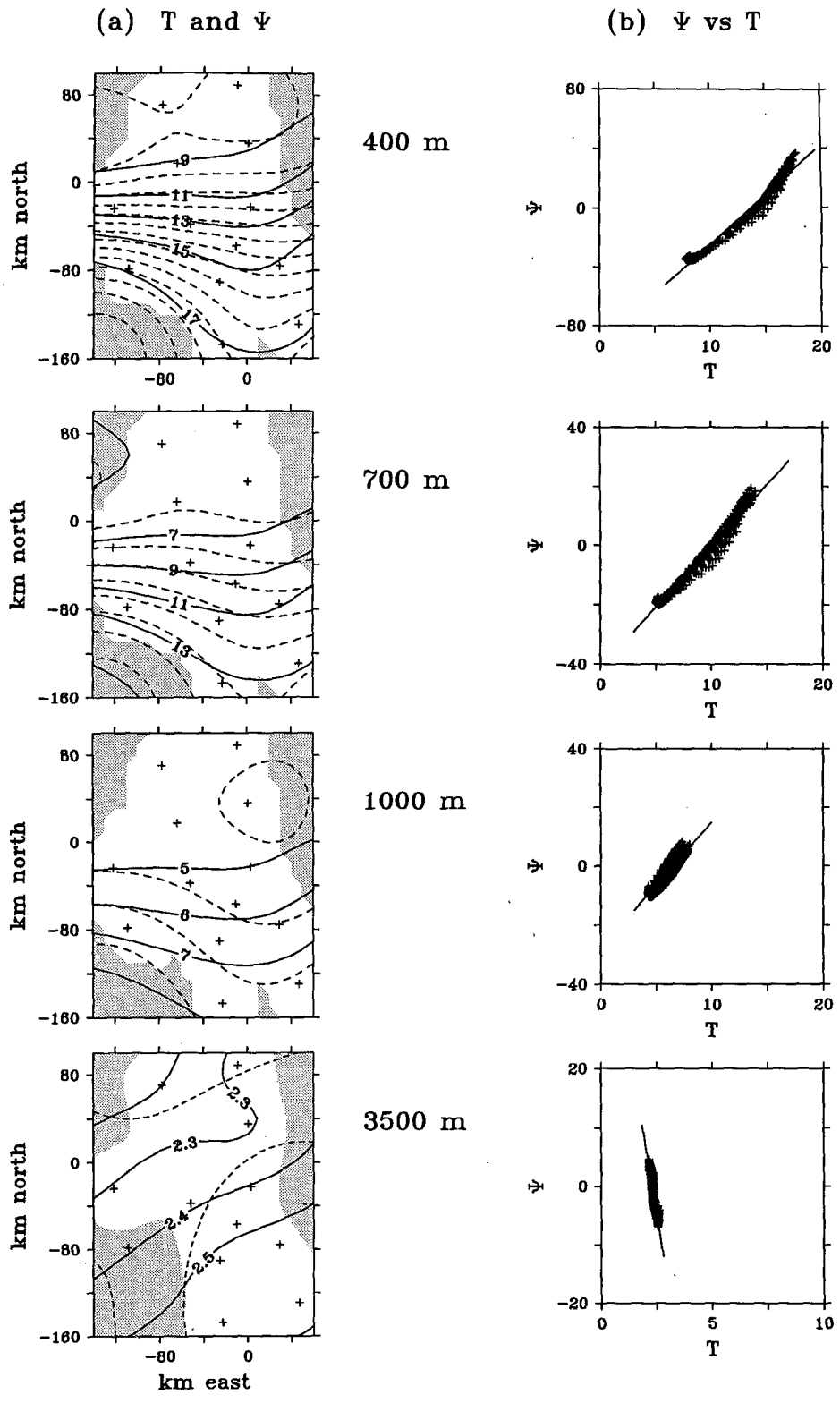


FIG. 3. (a) Maps of the mean temperature (solid) and mean streamlines (dashed) at 400, 700, 1000, and 3500 m. The lightly shaded regions have velocity error variances larger than 50% and the dark shaded regions have errors greater than 100%. (b) The scatterplots of the mean temperature and mean streamlines from the low-error (unshaded) region shown in (a); $d\bar{\psi}/d\bar{T}$ was estimated by fitting a straight line to the scatterplot.

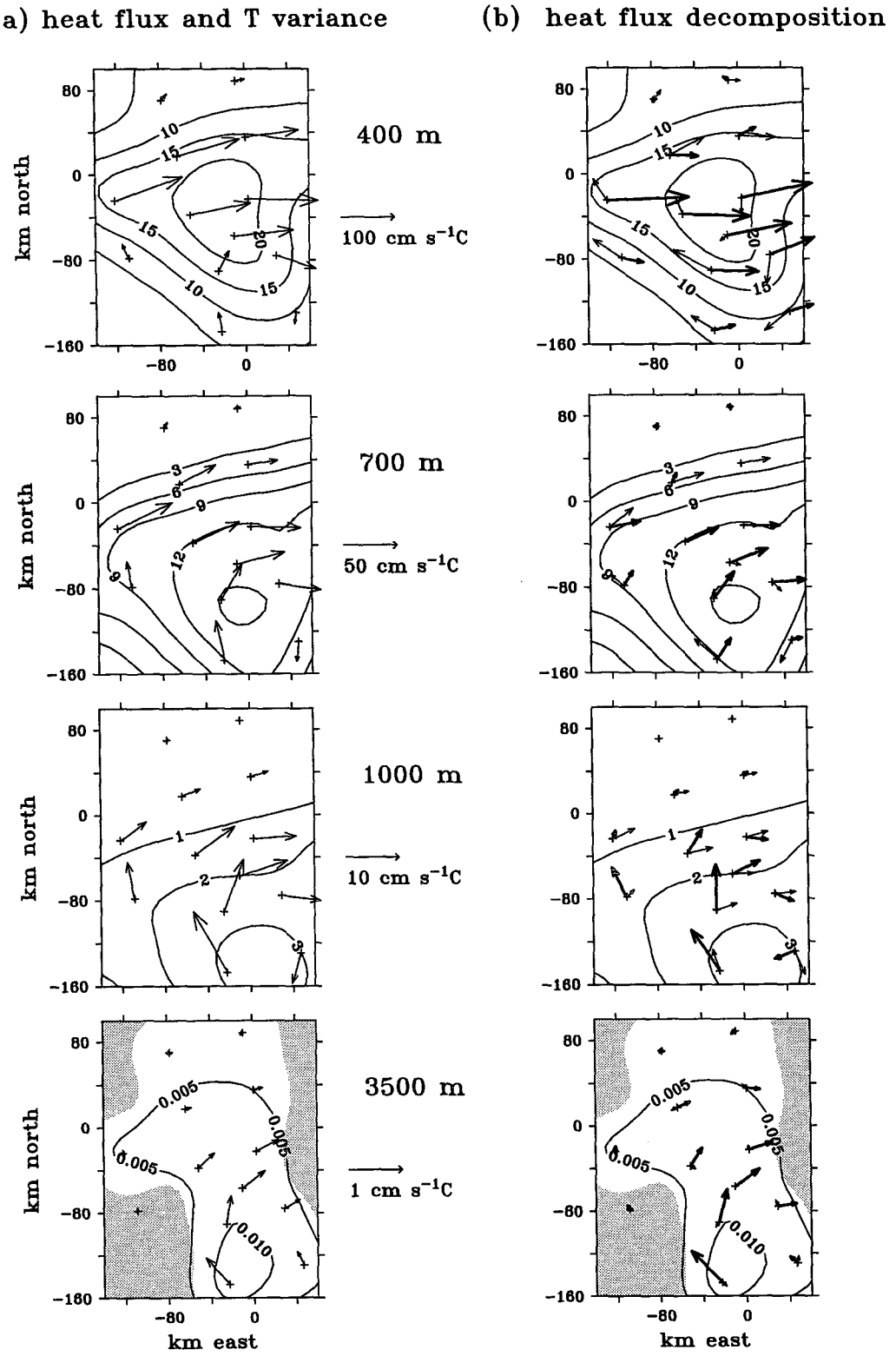


FIG. 4. (a) Heat flux vectors superimposed on maps of the temperature variance field. (b) The nondivergent (light) and residual divergent (dark) heat flux components superimposed on the temperature variance field. The nondivergent heat flux vectors, estimated using the Marshall and Shutts method, are always tangent to temperature variance contours. Together, the divergent and nondivergent components sum to be the total vector field shown in (a).

Figure 4 shows the full heat flux vectors and the horizontally divergent and nondivergent components superimposed upon the temperature variance contours. The temperature variance field has a local maximum centered along the trough axis in the mean temperature field. Because these variance contours are proportional to the streamlines of the nondivergent heat fluxes, the nondivergent component is always tangent to a temperature variance contour and is northward west of the trough axis, and southward east of the trough axis. The residual divergent eddy heat fluxes are indicative of eddy forcing due to the divergent eddy stretching flux. Because IESs were used to estimate $T$ at 400–1000 m around the periphery of the current meter array, the centered finite difference approximation of the temperature variance gradient [and therefore the heat flux decomposition (47)] can be applied everywhere within the current meter array.

### b. *Change in direction and speed of the mean current*

Figure 5a shows the mean geostrophic flow vectors $\bar{\mathbf{u}}$ superimposed on mean streamlines for each of the four levels (400, 700, 1000, and 3500 m). Near the trough axis where the radius of curvature in the upper-level mean flow is approximately 100 km, the centripetal acceleration $|\bar{\mathbf{u}}|^2/R$ is: $1.0 \times 10^{-4}$ cm s$^{-2}$ ($|\bar{\mathbf{u}}| \sim 40$ cm s$^{-1}$) at 400 m, $0.4 \times 10^{-4}$ cm s$^{-2}$ ($|\bar{\mathbf{u}}| \sim 30$ cm s$^{-1}$) at 700 m, and $0.1 \times 10^{-4}$ cm s$^{-2}$ ($|\bar{\mathbf{u}}| \sim 20$ cm s$^{-1}$) at 1000 m.

Due to the presence of the deep western boundary current, the deep mean flow is generally westward in the northern portion of the study region. However, surprisingly, as the westward deep flow crosses the trough axis, it is deflected southward into a permanent deep cyclone. The centripetal acceleration of the deep cyclone is approximately $0.03 \times 10^{-4}$ cm s$^{-2}$ ($|\bar{\mathbf{u}}| \sim 7$ cm s$^{-1}$, $R \sim 150$ km).

Notice that in the upper three levels, the speed (and therefore mean kinetic energy) is maximum at the western portion of the array, upstream of the trough axis. Thus, as can be seen in Fig. 5b, at these three levels, there is downstream deceleration: Contours of $\bar{\mathbf{u}} \cdot \nabla$MKE are negative. In contrast, at 3500 m, west of the trough axis, the downstream change in MKE appears to be positive: The deep mean flow tends to accelerate into the cyclone.

### c. $\mathbf{F}_{therm}$

Figure 6a shows the upper-layer, 700-m level, and deep-layer $\mathbf{F}_{\text{therm}}$ vectors superimposed on respectively the 400-, 700-, and 3500-m level mean streamlines. The two-layer upper and deep $\mathbf{F}_{\text{therm}}$ vectors are oriented in opposite directions, with the upper-layer $\mathbf{F}_{\text{therm}}$ oriented toward the northwest and the deep-layer $\mathbf{F}_{\text{therm}}$ oriented toward the southeast. This deep $\mathbf{F}_{\text{therm}}$ is oriented in the proper direction to accelerate and turn the deep western boundary current into a permanent deep cyclone beneath the upper-level trough axis. It is worth noting that the magnitude of the normal component of the deep $\mathbf{F}_{\text{therm}}$ is approximately 10 times larger than the centripetal acceleration, and likewise the rate of work done by the deep-layer $\mathbf{F}_{\text{therm}}$ is 10 times that necessary to achieve the observed rate of change in MKE.

The 700-m level $\mathbf{F}_{\text{therm}}$ is oriented to accelerate and turn the eastward flow southward almost everywhere. Because the mean flow is in fact observed to decelerate at 700 m, $\mathbf{F}_{\text{therm}}$ at this level must be nearly balanced by another term in the momentum budget.

Because the upper two-layer $\mathbf{F}_{\text{therm}}$ envoked unrealistic assumptions, it is not clear how realistic these vectors are. Nevertheless, it is interesting to note that the upper-layer $\mathbf{F}_{\text{therm}}$ is in the proper direction to cause the observed deceleration and cyclonic curvature at the trough axis.

### d. $\mathbf{F}_{mom}$

As can be seen in Fig. 7a, the pattern of $\mathbf{F}_{\text{mom}}$ vectors is vertically coherent, having a radial outward pattern along the trough axis at all levels. At the center of the trough, the pattern is clearly divergent and $\mathbf{F}_{\text{mom}}$ will enter the balanced (divergence) equation for the mean ageostrophic vorticity. Upstream of the trough, the radial pattern appears to be a certain degree nondivergent and therefore might be partially responsible for the deformation in the mean flow. In the deep layer, the radial outward pattern in $\mathbf{F}_{\text{mom}}$ tends to offset the cyclonic forcing by $\mathbf{F}_{\text{therm}}$. However, because the $\mathbf{F}_{\text{therm}}$ vectors are twice as large as the $\mathbf{F}_{\text{mom}}$ vectors, the net affect of the eddy forcing ($\mathbf{F}_{\text{therm}} + \mathbf{F}_{\text{mom}}$) is to induce a mean cyclonic circulation in the deep layer.

As can be seen in Fig. 7b, at all levels, $\mathbf{F}_{\text{mom}}$ tends to decelerate the mean flow. At 400 m, there is a near balance between the $W_{\text{mom}}$ and the downstream decrease in MKE. However with each deeper level, the misbalance between $W_{\text{mom}}$ (Fig. 7b) and the downstream change in MKE (Fig. 5b) increases. In the deep layer, $W_{\text{mom}} \sim -0.01 \times 10^{-3}$ cm$^2$ s$^{-3}$, while the downstream change in MKE is positive, approximately $+0.01 \times 10^{-3}$ cm$^2$ s$^{-3}$.

### e. $-\beta y \hat{\mathbf{z}} \times \bar{\mathbf{u}}$

The beta forcing only affects the normal component of the momentum budget and therefore can only change the direction of the mean flow. As can be seen in Fig. 8, in the southern portion of the array, the beta forcing tends to produce a cyclonic centripetal acceleration comparable in size to what is in fact observed at 700 m and deeper.

### f. $-f_0 \hat{\mathbf{z}} \times \tilde{\mathbf{u}}_a$

The residual ageostrophic flow $\tilde{\mathbf{u}}_a$ cannot be directly measured by the array. However, the misbalance be-

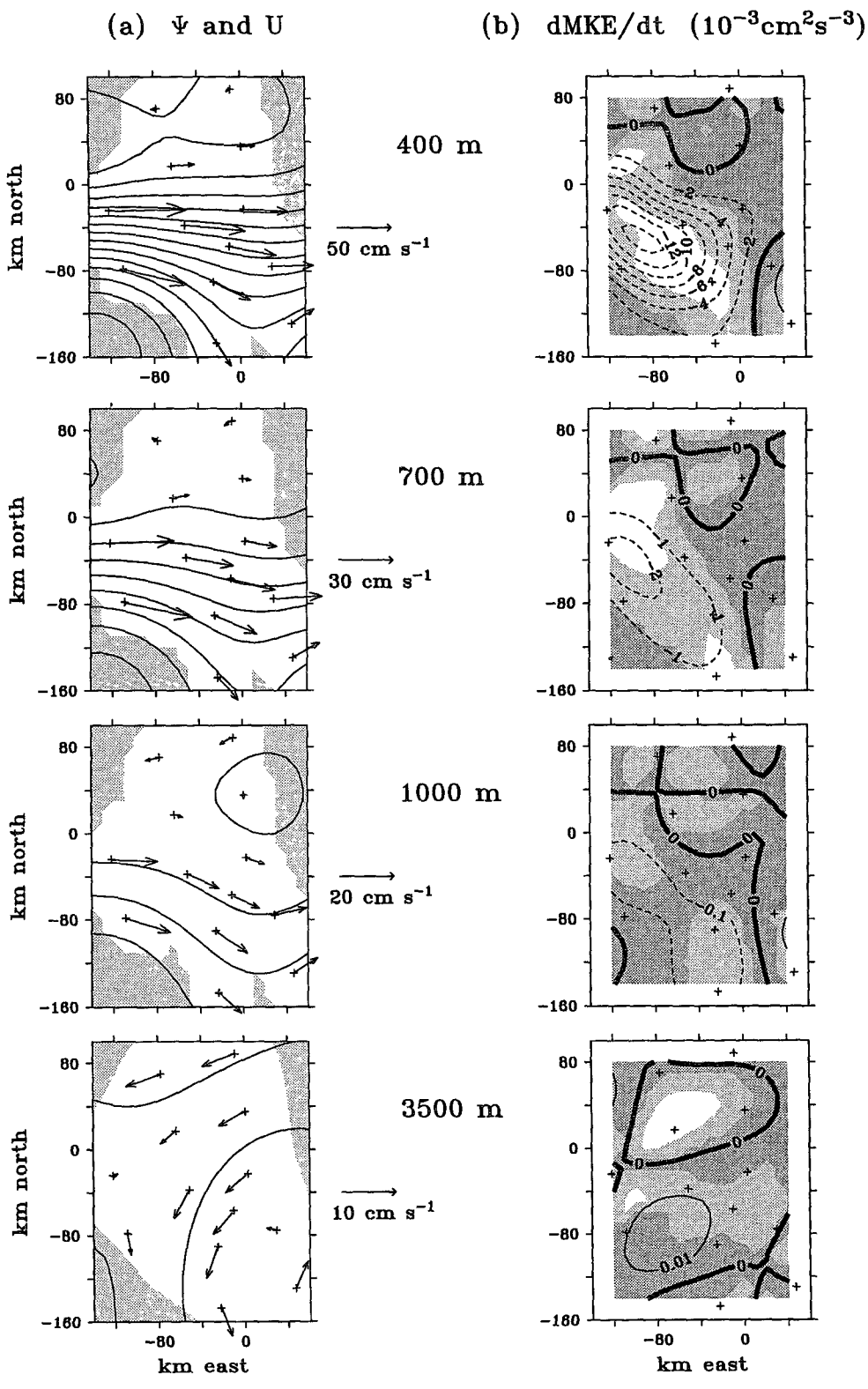


FIG. 5. (a) The mean flow vectors superimposed on maps of the mean streamlines. (b) Downstream change in the mean kinetic energy. The CI of the energetic terms in Figs. 5b and 7b are $2 \times 10^{-3}$ cm$^2$ s$^{-3}$, $1 \times 10^{-3}$ cm$^2$ s$^{-3}$, $0.1 \times 10^{-3}$ cm$^2$ s$^{-3}$, and $0.01 \times 10^{-3}$ cm$^2$ s$^{-3}$ for the levels 400, 700, 1000, and 3500 m. For all maps in Figs. 3–8, the lightly shaded regions have error variances larger than 50% and the dark shaded regions have errors greater than 100%.

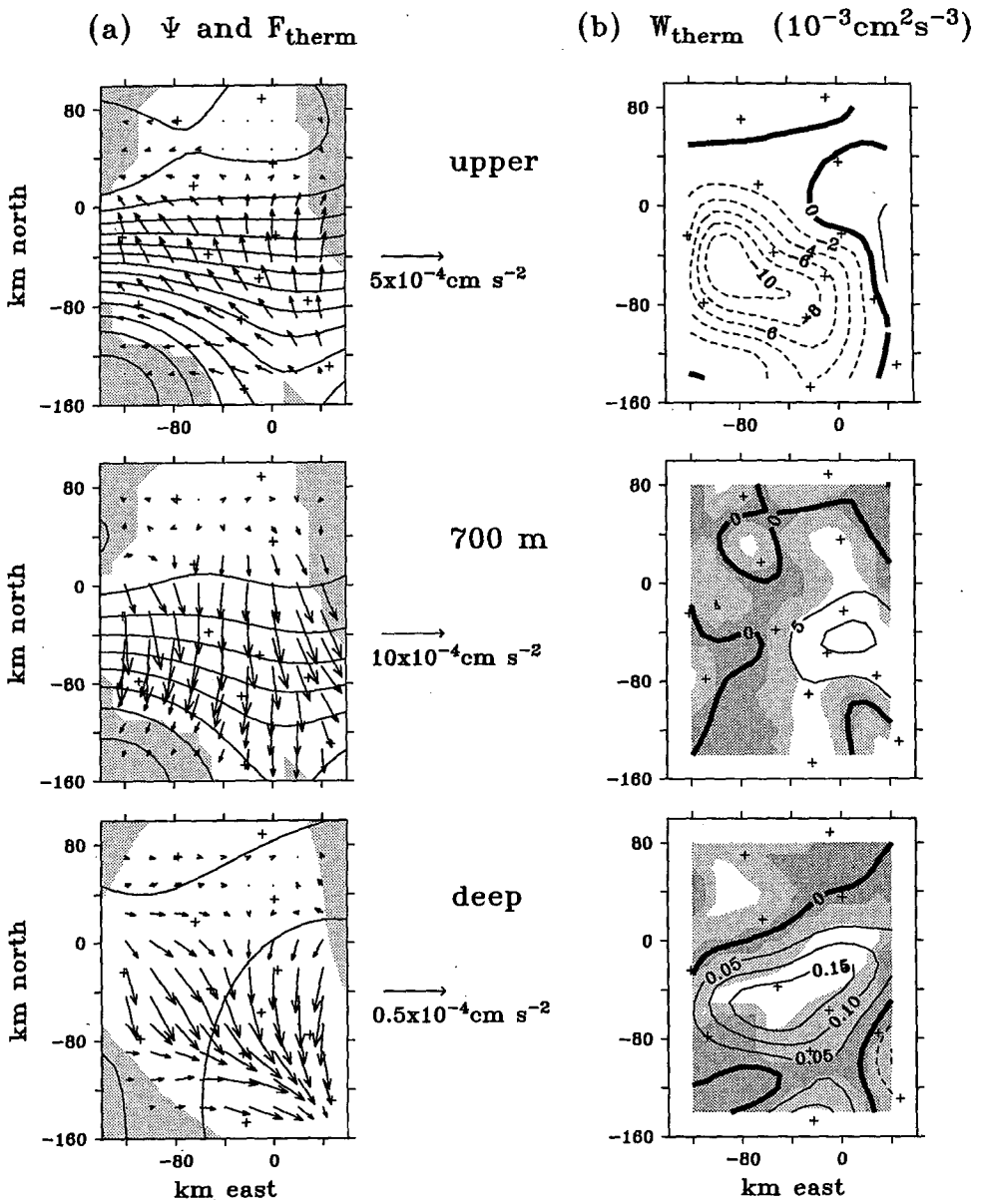


FIG. 6. (a) The $\mathbf{F}_{\text{therm}}$ vectors superimposed on the mean streamlines of flow, and (b) the rate of work done on the time-mean flow by $\mathbf{F}_{\text{therm}}$ ($W_{\text{therm}}$). The CI for $W_{\text{therm}}$ are $2 \times 10^{-3}$ cm$^2$ s$^{-3}$ for the upper two-layer approximation, $5 \times 10^{-3}$ cm$^2$ s$^{-3}$ at 700 m and $0.05 \times 10^{-3}$ cm$^2$ s$^{-3}$ for the deep layer. The upper and deep $\mathbf{F}_{\text{therm}}$ vectors were estimated with the two-layer assumption. Because this is a poor assumption in the upper level, no error field is estimated for the upper-level $W_{\text{therm}}$.

tween the observed forcing and the observed change in mean flow suggests that the Coriolis torque on the residual ageostrophic flow is important at all levels, and particularly at the 700-m level. At 700 m, the $\mathbf{F}_{\text{therm}}$ vectors are predominantly directed southward (normal to the mean flow), and are over an order of magnitude larger than $\mathbf{F}_{\text{mom}}$, the centripetal acceleration, and the beta forcing. Therefore, $\mathbf{F}_{\text{therm}}$ must be balanced to a large extent by the Coriolis torque on the residual ageostrophic flow at 700 m.

## 6. Discussion

A scale analysis shows that $\partial\bar{\mathbf{u}}/\partial t$ is several orders of magnitude smaller than the measured terms in the 26-month averaged momentum balance. Thus, the steady-state analysis is valid for these data. The large internal cancelation between $\mathbf{F}_{\text{therm}}$ and $-f_0\hat{\mathbf{z}} \times \tilde{\mathbf{u}}_a$ could be indicative of leakage of nondivergent heat fluxes into the residual "divergent" component, as discussed earlier in section 5a. However, we believe that there

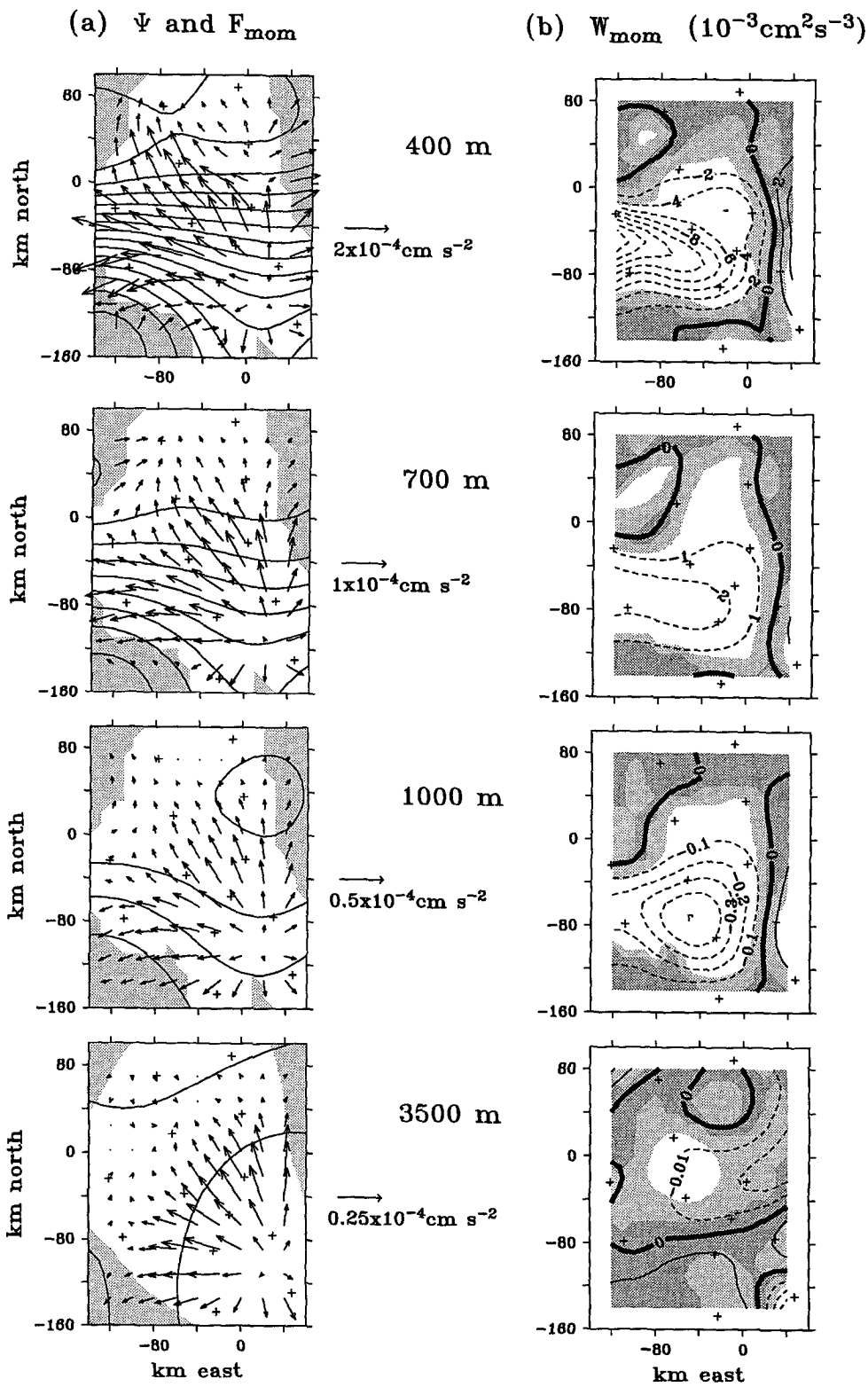


FIG. 7. (a) The $\mathbf{F}_{mom}$ vectors superimposed on the mean streamlines of flow, and (b) the rate of work done on the time-mean flow by $\mathbf{F}_{mom}$. CI as in Fig. 5.

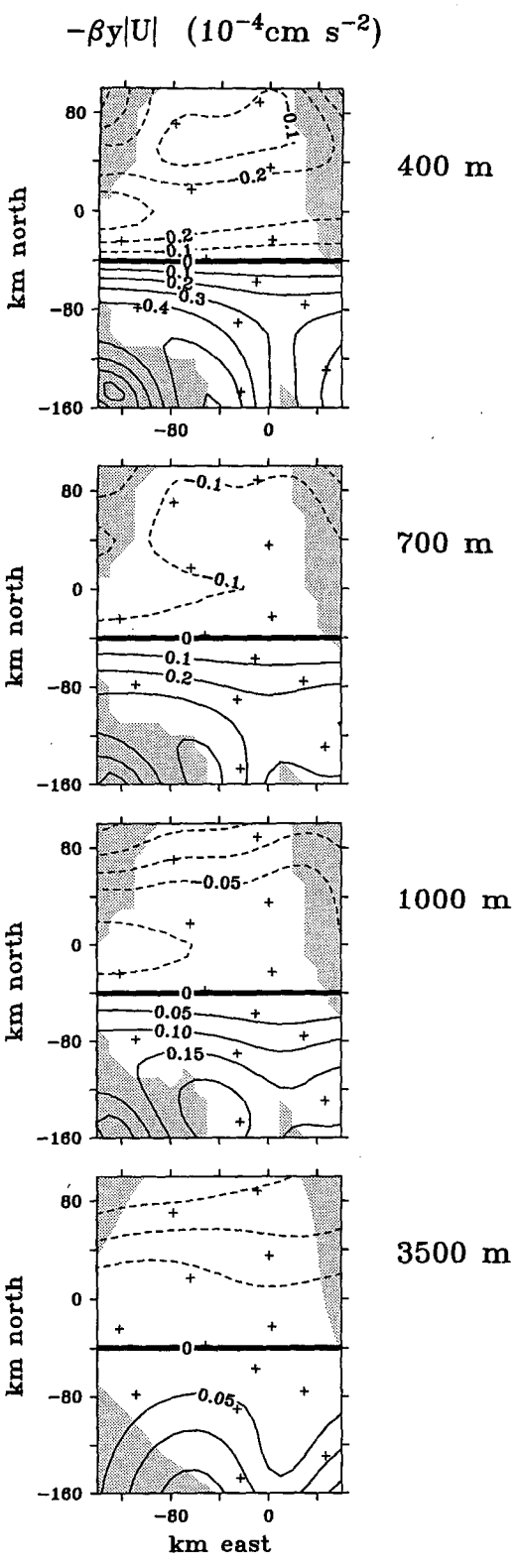


FIG. 8. Beta forcing contours in units of $10^{-4}$ cm s$^{-2}$. Positive contours induce a positive (cyclonic) mean centripetal acceleration.

are also dynamical justifications for such a balance at 700 m. Following the methodology of Bryden (1980) for estimating the vertical velocity profile from a single mooring, Hall (1986b) estimated the level of maximum vertical velocity to be 900 m at the 68°W GUSTO mooring. The level of maximum vertical velocity is equivalent to the level where the ageostrophic flow is horizontally nondivergent (lnd): $\partial w/\partial z = -\nabla\cdot\bar{\mathbf{u}}_a = 0$ at $z$ = lnd. Thus, at the level of nondivergence (i.e., maximum vertical velocity), $\bar{\mathbf{u}}_a^{\text{div}} \sim 0$ and by the definition of $\bar{\mathbf{u}}_a$ (28), $\mathbf{F}_{\text{therm}}$ must balance the Coriolis torque on the divergent component of the residual ageostrophic flow

$$-f_0\hat{\mathbf{z}}\times\bar{\mathbf{u}}_a^{\text{div}}|_{z=\text{lnd}} = (-f_0\hat{\mathbf{z}}\times\tilde{\mathbf{u}}_a^{\text{div}} + \mathbf{F}_{\text{therm}})|_{a=\text{lnd}} = 0.$$

The 700-m level $\mathbf{F}_{\text{therm}}$ shown in Fig. 6a is estimated using a vertical finite difference range of 400–1000 m, which spans the level of nondivergence as measured by Hall (1986b). Thus, the large cancelation between $\mathbf{F}_{\text{therm}}$ and $-f_0\hat{\mathbf{z}}\times\tilde{\mathbf{u}}_a$ at 700 m could be caused by ocean dynamics at the level of nondivergence, and/or by leakage of nondivergent heat fluxes into the residual divergent component.

Assuming a rigid thermocline structure to bin the flow covariance $\overline{u'v'}$ measured by the 68°W GUSTO mooring into cyclonic and anticyclonic sides of the stream, Hall (1986a) shows that the flux divergence $(\overline{u'v'})_y$ tends to decelerate the mean flow above 900 m and accelerate the mean flow below 900 m. In contrast, our analysis suggests that $\mathbf{F}_{\text{mom}}$ tends to decelerate the flow throughout the water column at 68°W. As can be seen from the variance ellipses shown in Fig. 11a of Part I, neglecting $(\overline{u'u'})_x$ can lead to a serious underestimation of $\mathbf{F}_{\text{mom}}$ at 68°W and could account for the discrepancies between the results of the two analyses.

Upstream of the study region, at 73°W, Dewar and Bane (1989) estimate the mean kinetic energy budget on the anticyclonic side of the mean Gulf Stream using data from a cluster of five tall current meter moorings. Their analysis shows that at 380 and 500 m above the bottom, the Reynold stresses ($\mathbf{F}_{\text{mom}}$) accelerate the mean flow, while at 880 and 1880 m, the Reynold stresses decelerate the mean flow. Unlike at 68°W, where for 400–1000 m there is a near balance between the downstream change in MKE and $W_{\text{mom}}$, at 73°W these terms have opposite signs at all levels. Therefore, the inferred mean pressure work is important at all levels and is upgradient at 380 and near the bottom, and downgradient at 880 m and 1880 m. Dewar and Bane therefore conclude that the mean flow at 73°W is predominately inertial and that the pressure minimum shifts with depth. In view of the fact that $W_{\text{therm}}$ is contained within their mean pressure work term (i.e., $\mathbf{F}_{\text{therm}}$ is contained in the ageostrophic Coriolis torque), it is perhaps misleading to claim that the steady-state dynamics at 73°W are predominately inertial rather than eddy forced.

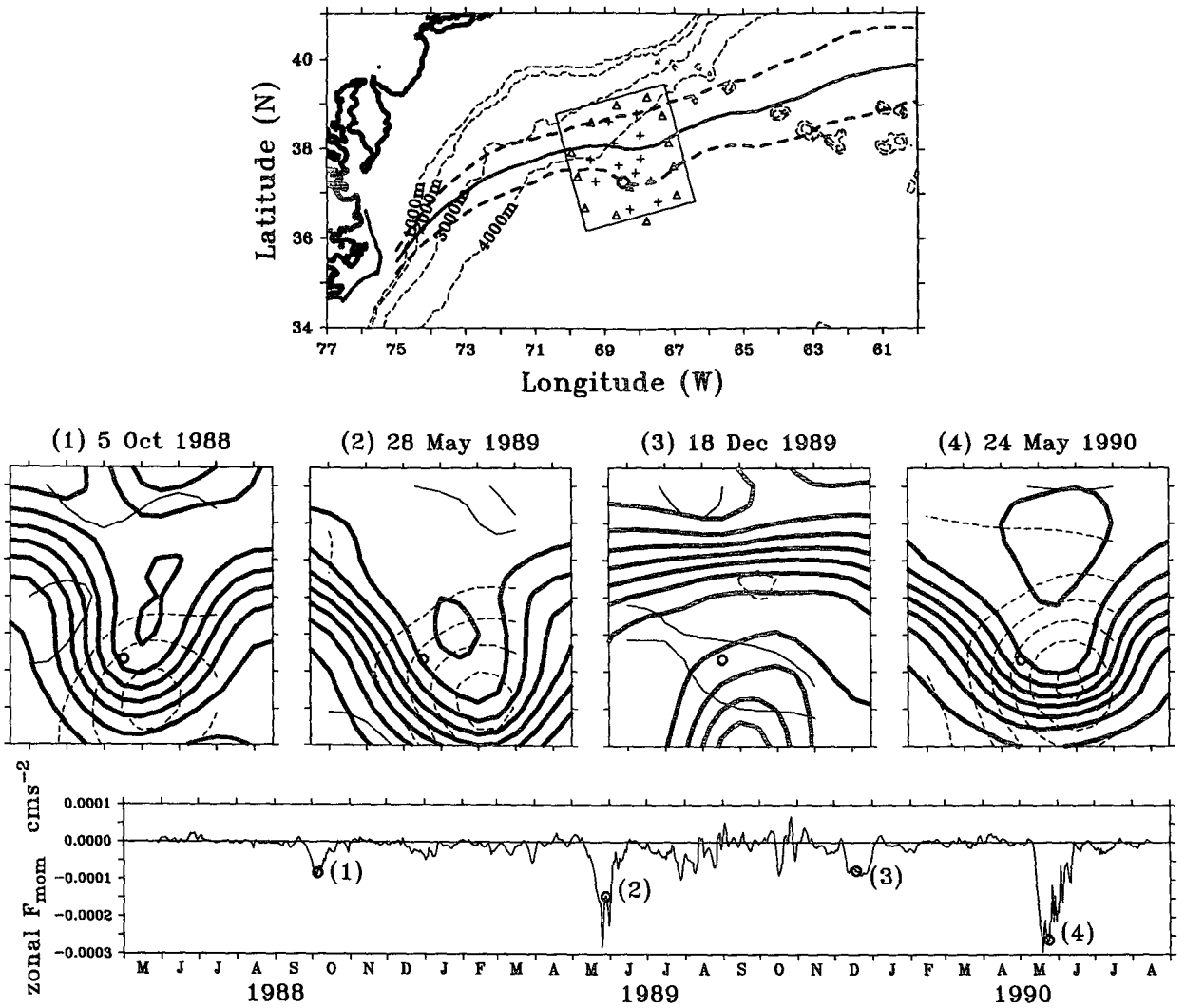


FIG. 9. The 3500-m level $\mathbf{F}_{mom} \cdot \hat{\mathbf{x}} = -\partial(u'u')/\partial x - \partial(u'v')/\partial y$ time series at (37.28°N, 68.46°W) [(−80, −40) km in the north/east coordinate system in Figs. 3–8]. The location is shown as an open circle in the selected contour maps of the IES thermocline topography (dark contours) and 3500-m dynamic pressure (light contours). The IES thermocline topography can be interpreted as baroclinic streamlines of flow. The deep dynamic pressure contours can be interpreted as 3500-m level streamlines, with dashed contours representing low pressure anomalies. Major peaks in the $\mathbf{F}_{mom} \cdot \hat{\mathbf{x}}$ time series can be associated with cold core ring stream interactions and trough events that extend through the entire water column.

While the meanders at 73°W tend to grow in amplitude as they propagate downstream (Watts 1983; Kontoyiannis and Watts 1994), at 68°W there is a tendency for troughs to stall and experience their full life cycle of growth and decay locally (Watts et al. 1995). During the 26-month experiment, six steep troughs formed in the study region, with each event lasting approximately a month. As discussed in Part I, the eddy energetics suggest that these events are caused by baroclinic instability. One might wonder therefore if the eddy forces shown in Figs. 6–7 are characteristic of eddies generated by baroclinic instability.

The effect of nonlinear baroclinic instability waves on the zonal-mean flow has been studied by Simmons and Hoskins (1978) and Edmon et al. (1980). In these nonlinear baroclinic instability life cycle experiments, the time evolution of the zonal-mean EP fluxes show thermal forcing in the growth stage and momentum flux forcing in the decay stages. We argue that a similar result holds for the time-mean Gulf Stream flow at 68°W: The $\mathbf{F}_{therm}$ patterns in Fig. 6 are consistent with the growth stage of the trough formation events, and the $\mathbf{F}_{mom}$ patterns in Fig. 7 are consistent with the decay stage.

The life cycle of a typical baroclinic midlatitude storm is described by Wallace and Hobbs (1977, see Fig. 3.22, p. 139): During the initial growth stage, a (bottom) surface low-pressure perturbation develops

downstream of an upper-level trough, causing the streamlines to tilt westward with height. By thermal wind, this geometry is associated with warm (cold) advection into the upper-level meander crest (trough), which then amplifies the upper-level meander. The vertical motion associated with warm advection spins up and intensifies the deep low pressure cyclone downstream of the upper-level trough, which further amplifies the upper-level meander.

In Fig. 16 of Part I, each trough event can be associated with a peak in the 700-m level divergent heat flux time series. These divergent heat fluxes can be associated with divergent stretching fluxes, and as can be seen in Fig. 6a, the $\mathbf{F}_{\text{therm}}$ vectors are clearly oriented to "spin up" a deep-layer cyclone and amplify the upper-level trough. The observed $\mathbf{F}_{\text{therm}}$ are therefore consistent with the initial growth stage of a typical baroclinic self-development event.

In the decay stage of the typical life cycle, the center of the deep low pressure becomes aligned with the upper-level trough axis, eliminating the heat advection and causing the flow to become nearly barotropic. Momentum fluxes eventually radiate the energy away, causing the barotropic cyclone to dissipate. Figure 9 shows the time series of the zonal component of the 3500-m level $\mathbf{F}_{\text{mom}}$ vector at (37.28°N, 68.46°W), that is, $(-80, -40)$ km in the north/east coordinate system in Figs. 5–8. Each peak in this $\mathbf{F}_{\text{mom}}$ time series can be associated with either a cold core ring–stream interaction or the decay stage of a deep trough event when the upper level trough field and the deep cyclone are vertically aligned. Thus, the vertically coherent, radial pattern of $\mathbf{F}_{\text{mom}}$ is consistent with the decay (spin down) stage of a baroclinic self-development life cycle.

This analysis illustrates a classic example of eddy–mean flow interaction whereby eddies, generated by a baroclinically unstable mean jet, act back on the mean flow to make the flow more barotropic (i.e., stable) by spinning up and accelerating the deep-layer flow. A similar phenomena can be seen in eddy-resolving models of the North Atlantic (Holland and Rhines 1980; Harrison 1982): Instabilities occurring on a westward branch of the recirculation gyre are associated with heat fluxes and vortex stretching that produce a deep-layer turbulent Sverdrup balance that spins up deep recirculation gyres.

The theory of eddy forced quasigeostrophic time-mean flow presented here provides a formal correspondence between potential vorticity analyses and momentum analyses. A divergence in the eddy potential vorticity flux field corresponds to eddy forces that can change the speed and direction of the time-mean flow. These eddy forces can be evaluated from measurements of the three-dimensional structure of the horizontal eddy momentum fluxes and divergent heat flux fields. The Marshall and Shutts (1981) method of estimating the divergent heat fluxes appears to be robust, giving a (thermal) eddy force at 68°W, consistent with the growth stage of a nonlinear baroclinic instability event. The eddy force due to the eddy momentum fluxes at 68°W is consistent with the decay stage of the baroclinic instability life cycle.

*Acknowledgments.* This work was supported by the NSF Grant OCE87-17144 and ONR Contracts N00014-90-J-1568, N00014-90-J-1548, and N00014-92-J-4013 to Dr. D. R. Watts at the University of Rhode Island. Revisions were made at NOAA/PMEL, while the author was funded by a NOAA postdoctoral fellowship in Climate and Global Change, a program administered by UCAR. D. R. Watts, L. M. Rothstein, H. T. Rossby, J. M. Bane, L. Thompson, D. E. Harrison, and two anonymous reviewers made helpful comments on various incarnations of the manuscript. The author also wishes to thank John Marshall for an inspiring discussion about divergent heat fluxes, Tom Shay for processing the current meter data, Xiaoshu Qian and Nelson Hogg for their help and guidance in creating the gridded fields, and Randy Watts for invaluable discussions of the work.

## REFERENCES

Andrews, D. G., 1990: On the forcing of time-mean flows by transient, small amplitude eddies. *J. Atmos. Sci.*, **47,** 1837–1844.

——, and M. E. McIntyre, 1976: Planetary waves in horizontal and vertical shear: The generalized Eliassen–Palm relation and the mean zonal acceleration. *J. Atmos. Sci.*, **33,** 2031–2048.

Bluestein, H. B., 1992: *Synoptic–Dynamic Meteorology in Midlatitudes.* Vol. 1. Oxford University Press, 431 pp.

Bretherton, F. P., R. E. Davis, and C. B. Fandry, 1976: A technique for objective analysis and design of oceanographic experiments applied to MODE-73. *Deep-Sea Res.*, **23,** 559–582.

Bryden, H. L., 1980: Geostrophic vorticity balance in midocean. *J. Geophys. Res.*, **85,** 2825–2828.

Chester, D., P. Malanotte-Rizzoli, J. Lynch, and C. Wunsch, 1994: The eddy radiation field of the Gulf Stream as measured by ocean acoustic tomography. *Geophys. Res. Lett.*, in press.

Cornillon, P., 1986: The effect of the New England Seamounts on Gulf Stream meandering as observed from satellite IR imagery. *J. Phys. Oceanogr.*, **16,** 386–389.

Cronin, M., and D. R. Watts, 1996: Eddy-mean flow interaction in the Gulf Stream at 68°W. Part I: Eddy energetics. *J. Phys. Oceanogr.*, **26,** 2107–2131.

——, K. L. Tracey, and D. R. Watts, 1992: Mooring motion correction of the SYNOP Central Array current meter data, Tech. Rep. 92-4, University of Rhode Island, Kingston, RI, 114 pp.

Dewar, W. K., and J. M. Bane, 1989: Gulf Stream dynamics. Part I: Mean flow dynamics at 73°W. *J. Phys. Oceanogr.*, **19,** 1558–1573.

Edmon, H. J., Jr., B. J. Hoskins, and M. E. McIntyre, 1980: Eliassen–Palm cross sections for the troposphere. *J. Atmos. Sci.*, **37,** 2600–2616.

Gill, A. E., 1982: *Atmosphere–Ocean Dynamics.* Academic Press, 662 pp.

Hall, M. M., 1986a: Assessing the energetics and dynamics of the Gulf Stream at 68°W from moored current measurements. *J. Mar. Res.*, **44,** 423–443.

——, 1986b: Horizontal and vertical structure of the Gulf Stream velocity field at 68°W. *J. Phys. Oceanogr.*, **16,** 1814–1828.

——, and N. Fofonoff, 1993: Downstream development of the Gulf Stream from 68°W to 55°W. *J. Phys. Oceanogr.*, **23,** 225–249.

Halliwell, G. R., Jr., and C. N. K. Mooers, 1983: Meanders of the Gulf Stream downstream from Cape Hatteras 1975–1978. *J. Phys. Oceanogr.*, **13,** 1275–1292.

Harrison, D. E., 1982: On deep mean flow generation mechanisms and the abyssal circulation of numerical model gyres. *Dyn. Atmos. Oceans,* **3,** 289–325.

Hogg, N. G., 1991: Mooring motion corrections revisited. *J. Atmos. Oceanic Technol.,* **8,** 289–295.

——, 1992: On the transport of the Gulf Stream between Cape Hatteras and the Grand Banks. *Deep-Sea Res.,* **39,** 1231–1246.

Holland, W. R., and P. B. Rhines, 1980: An example of eddy-induced ocean circulation. *J. Phys. Oceanogr.,* **10,** 1010–1031.

Holopainen, E., 1984: Statistical local effect of synoptic-scale transient eddies on the time-mean flow in the northern extratropics in winter. *J. Atmos. Sci.,* **41,** 2505–2515.

Holton, J. R., 1992: *An Introduction to Dynamic Meteorology.* 3d ed. Academic Press, 511 pp.

Hoskins, B. J., 1983: Modelling of the transient eddies and their feedback on the mean flow. *Large-Scale Dynamical Processes in the Atmosphere,* B. Hoskins and R. Pearce, Eds., Academic Press, 169–199.

——, I. N. James, and G. H. White, 1983: The shape, propagation, and mean–flow interaction of large-scale weather systems. *J. Atmos. Sci.,* **40,** 1595–1612.

Kontoyiannis, H., and D. R. Watts, 1994: Observations on the variability of the Gulf Stream path between 74°W and 70°W. *J. Phys. Oceanogr.,* **24,** 1999–2013.

Lee, T., 1994: Variability of the Gulf Stream path observed from satellite infrared images. Ph.D. dissertation, University of Rhode Island, 188 pp.

Marshall, J., and G. Shutts, 1981: A note on rotational and divergent eddy fluxes. *J. Phys. Oceanogr.,* **11,** 1677–1680.

Plumb, R. A., 1986: Three-dimensional propagation of transient quasi-geostrophic eddies and its relationship with the eddy forcing of the time-mean flow. *J. Atmos. Sci.,* **43,** 1657–1678.

Rhines, P. B., and W. R. Holland, 1980: A theoretical discussion of eddy-driven mean flows. *Dyn. Atmos. Oceans,* **3,** 289–325.

Shay, T. J., S. M. Haines, J. M. Bane, and D. R. Watts, 1994: SYNOP Central Array current meter data report: Mooring period May 1988–September 1990. University of North Carolina Tech. Rep. CMS 91-2, 106 pp.

——, J. M. Bane, D. R. Watts, and K. L. Tracey, 1995: Gulf Stream flow field and events near 68°W. *J. Geophys. Res.,* **100,** 22 565–22 589.

Simmons, A. J., and M. J. Hoskins, 1978: The life cycles of some nonlinear baroclinic waves. *J. Atmos. Sci.,* **35,** 414–432.

Tracey, K. L., and D. R. Watts, 1991: The SYNOP experiment: Thermocline depth maps for the Central Array October 1987 to August 1990. GSO Tech. Rep. 91-5, University of Rhode Island, Kingston, RI, 193 pp.

Trenberth, K. E., 1986: An assessment of the impact of transient eddies on the zonal flow during a blocking episode using localized Eliassen–Palm flux diagnostics. *J. Atmos. Sci.,* **43,** 2070–2087.

Wallace, J. M., and P. V. Hobbs, 1977: *Atmospheric Science. An Introductory Survey.* Academic Press, 467 pp.

Watts, D. R., 1983: Gulf Stream variability. *Eddies in Marine Science,* A. R. Robinson, Ed., Springer-Verlag, 114–144.

——, J. M. Bane, K. L. Tracey, and T. J. Shay, 1995: Gulf Stream path and thermocline structure near 74°W and 65°W. *J. Geophys. Res.,* **100,** 18 291–18 312.

White, F. M., 1974: *Viscous Fluid Flow.* McGraw-Hill, 725 pp.